Modelling the radiative effects of biomass burning aerosols on carbon fluxes in the Amazon region

Demerval S. Moreira[1,2], Karla M. Longo[3,a], Saulo R. Freitas[3,a], Marcia A. Yamasoe[4], Lina M. Mercado[5,6], Nilton E. Rosário[7], Emauel Gloor[8], Rosane S. M. Viana[9], John B. Miller[10], Luciana V. Gatti[11,12], Kenia T. Wiedemann[13], Lucas K. G. Domingues[11,12], and Caio C. S. Correia[11,12]

[1]Universidade Estadual Paulista (Unesp), Faculdade de Ciências, Bauru, SP, Brazil.
[2]Centro de Meteorologia de Bauru (IPMet), Bauru, SP, Brazil.
[3]Centro de Previsão de Tempo e Estudos Climáticos, Instituto Nacional de Pesquisas Espaciais (INPE), Cachoeira Paulista, SP, Brazil.
[4]Departamento de Ciências Atmosféricas do Instituto de Astronomia, Geofísica e Ciências Atmosféricas, Universidade de *São Paulo* (USP), *São Paulo*, SP, Brazil.
[5]Geography, College of Life and Environmental Sciences, University of Exeter, Exeter, UK.
[6]Centre for Ecology and Hydrology (CEH), Wallingford, UK.
[7]Universidade Federal de *São Paulo* (UNIFESP), Campus Diadema, Diadema, SP, Brasil.
[8]School of Geography, University of Leeds, Woodhouse Lane, Leeds, UK.
[9]Departamento de Matemática, Universidade Federal de Viçosa (UFV), Viçosa, MG, Brazil.
[10]Global Monitoring Division, Earth System Research Laboratory, National Oceanic and Atmospheric Administration (NOAA), Boulder, Colorado 80305, USA.
[11]Centro de Ciências do Sistema Terrestre, Instituto Nacional de Pesquisas Espaciais (INPE), São José dos Campos, SP, Brazil.
[12]Instituto de Pesquisas Energéticas e Nucleares (IPEN) – Comissão Nacional de Energia Nuclear (CNEN), São Paulo, Brazil.
[13]Department of Ecology and Evolutionary Biology, University of Arizona, Tucson, AZ, USA.
[a]Now at Universities Space Research Association/Goddard Earth Sciences Technology and Research (USRA/GESTAR) at Global Modeling and Assimilation Office, NASA Goddard Space Flight Center, Greenbelt, MD, USA.

Correspondence to: Demerval S. Moreira (demerval@fc.unesp.br)

Abstract. Every year, a dense smoke haze covers a large portion of South America originating from fires in the Amazon Basin and central parts of Brazil during the dry/biomass-burning season between August and October. Over a large portion of South America, the average aerosol optical depth at 550 nm exceeds 1.0 during the fire season while the background value during the rainy season is below 0.2. Biomass burning aerosol particles increase scattering and absorption of the incident solar radiation. The regional-scale aerosol layer reduces the amount of solar energy reaching the surface, cools the near surface air, and increases the diffuse radiation fraction over a large disturbed area of the Amazon rainforest. These factors affect the energy and CO_2 fluxes at the surface. In this work, we applied a fully integrated atmospheric model to assess the impact of biomass burning aerosols in CO_2 fluxes in the Amazon region during 2010. We address the effects of the attenuation of the global solar radiation and the enhancement of the diffuse solar radiation flux inside the vegetation canopy. Our results indicate that the biomass burning aerosols led to increases of about 27% of gross primary productivity of *Amazônia*, 10% of plant respiration and a decline in soil respiration of 3%. Consequently, in our model *Amazônia* became a net carbon sink; net ecosystem exchange during September 2010 dropped from +101 to -104 TgC when the aerosol effects are considered, mainly

due to the aerosol diffuse radiation effect. For the forest biome, our results point to a dominance of the diffuse radiation effect on CO_2 fluxes, reaching a balance of 50% – 50% between the diffuse and direct aerosol effects for high aerosol loads. For C3 grasses and Savanna (*cerrado*), as expected, the contribution of the diffuse radiation effect is much lower, tending to zero with the increase of aerosol load. Taking all biomes together, our model shows the Amazon during the dry season, in the presence of high biomass burning aerosol loads, changing from being a source to being a sink of CO_2 to the atmosphere.

1 Introduction

The austral winter in most of South America is typically dry with extensive vegetation fires, mostly human induced, in areas of deforestation and agricultural/pasture land management. The fire activity, especially in *Amazônia* and *cerrado* areas (a savanna-like biome), usually last for at least 3 months, from August to October every year, and has been typically called "biomass burning season". Fire emissions can be a significant source of carbon dioxide (CO_2) to the atmosphere [e.g., Gatti, 2014], and a major source of several other trace gases to the atmosphere (Andreae et al., 2002). In addition to trace gases, vegetation fires also produce a large amount of aerosol particles, in particular in the fine mode, which, on average, contribute to at least 90% of the total AOD in the visible spectrum in the case of the South America regional smoke (Reid et al., 2005; Rosário, 2011). The resulting smoke haze typically covers areas of several millions of km^2 over South America (Prins et al., 1998). Outside the biomass burning season, mean AOD in the visible spectrum varies from 0.10 to 0.15 across the Amazon rainforest, and from 0.12 to 0.20 in the *cerrado* areas (Schafer et al., 2008; Rosario, 2011). At the peak of the burning season, during September, monthly mean AOD can reach values up to 10 and 5 times higher than the clean wet season values in the southern and the northern areas, respectively (Schafer et al., 2008; Rosário, 2011). The Ångström exponent (AE), an optical property used to characterize aerosol particle size based on the spectral dependence of AOD, increases from 0.60, during the clean period, to 2.0 during the peak of the burning season (Schafer et al., 2008). Such high value of AE is representative of air masses dominated by fine mode particles, a major feature of the South American regional plume. Low values of AE indicate dominance of coarse mode particles, a characteristic of the pristine region of the Amazon dominated by biogenic particles. The absorption characteristics of the particles, expressed by the optical property Single Scattering Albedo (SSA), ranges in the southern portion of Amazon forest during burning season from 0.92-0.93 at 550 nm and reveals a dominance of moderate absorbing particles (Schafer et al., 2008), unlike those from *cerrado*, which are highly absorbing and present low value of SSA (0.89±0.04). The *cerrado* has substantially lower SSA than the mean values in the southern Amazon forest due to the higher fraction of flaming phase combustion, typical of savanna-like vegetation (Schafer et al., 2008).

In *Amazônia* under heavy smoke conditions, the surface cooling can reach 3° C, restraining the turbulent flows and consequently the evapotranspiration of water and sensible heat flux. Thus, the result is a drier and shallower boundary layer, inhibiting formation/development of convective clouds and hence decreasing precipitation (Yu et al., 2002). In particular, biomass burning aerosols reduces the net direct solar radiation reaching the surface while it increases the diffuse fraction of solar radiation. The diffuse fraction of the photosynthetically active radiation (PAR) can increase from about 19%, which is the typical value for a clean atmosphere scenario, up to 80% under biomass burning conditions (Yamasoe, et al., 2006). Biomass burning aerosols

also act as cloud condensation nuclei affecting cloud microphysical properties and therefore change the radiation budget and hydrological cycle over disturbed areas (Kaufman, 1995; Rosenfeld, 1999; Andreae, et al., 2004; Koren et al., 2004).

Changes in the total downward solar irradiance at the surface usually does not impact the photosynthetic activity of the leaves on the top of the forest canopy because those are usually light saturated around midday, closing the plants' stomata. On the other hand, sub-canopy leaves remain typically under light-deficit conditions and do not fully achieve their photosynthetic potential. Thus, increasing the diffuse light, which penetrates deeper into the canopy, increases PAR availability to the sub-canopy leaves and the rate of photosynthesis, and consequently atmospheric carbon assimilation (Baldocchi, 1997; Misson et al., 2005; Oliveira et al., 2007; Knohl and Baldocchi, 2008; Mercado et al., 2009; Doughty et al., 2010; Kanniah et al., 2012; Rap et al., 2015). However, the increase of the diffuse radiation is also accompanied by a decrease in the total radiation, therefore defining an optimal diffuse to total radiation fraction that allows a maximum of carbon assimilation. Under heavy pollution or cloudy skies, plant productivity increases with the diffuse radiation, though it is still insufficient to compensate the reduction of the total irradiance reaching the surface. Additionally, other authors suggest that the contribution of biomass burning aerosols on CO_2 assimilation can also be due to the cooling of the air (Min, 2005; Doughty et al., 2010; Steiner and Chameides, 2011), causing an increase of relative humidity (Collatz et al., 1991) near the earth's surface, which reduces plant respiration and thermal stress of the leaves. Indeed, field observations indicate that tropical forest productivity is highly sensitive to temperature variations (Feeley et al., 2007), with CO_2 assimilation decreasing sharply during warmer periods. Doughty et al. (2010) estimated that under dense, biomass burning conditions in *Amazônia*, 80% of the increase of CO_2 absorption is due to the increase of sub-canopy light (diffuse radiation) and only 20% is due to the reduction of the canopy temperature. The Gross Primary Production (GPP) is the total carbon uptake resulting from photosynthesis by plants, especially leaves, in an ecosystem over a land area. GPP responds to the amount of photosynthetically active radiation portion of solar energy reaching the plants, given limitations of soil moisture and nutrients. A modeling study at the global scale exploring the aerosol impact on GPP concluded that the positive effect of the diffuse radiation increase was indeed larger than the negative effect of the irradiance reduction (Mercado et al., 2009). JULES simulations forced with aerosol fields from the Hadley Centre Global Environment Model version 2 (HadGEM2) made by these authors pointed to an increase in the diffuse fraction of irradiance, and a consequent increase in the global carbon uptake of 23.7% from 1960 to 1999. Rap et al. (2015) also using JULES, but with a different off-line aerosol model – 3-D GLObal Model of Aerosol Processes (GLOMAP, Mann et al., 2010), estimated that the biomass burning aerosols affected the diffuse radiation by 3.4 to 6.8% and increased the net primary production (NPP) of 1.4 to 2.8% in *Amazônia* during the period between 1998 and 2007. Besides, the biomass burning aerosol indirect effect will also impact the CO_2 fluxes by changing the amount of rain (and soil moisture), and solar radiation availability and diffuse fraction. Lastly, vegetation fires also emit ozone precursors and promote tropospheric ozone production, and surface deposition. Ozone is highly phytotoxic, damaging plants stomata and reducing CO_2 uptake (Sitch et al., 2007).

Motivated by all these previously cited recent observational and theoretical studies that have demonstrated the impacts of aerosols on the CO_2 fluxes, we applied an integrated in-line numerical atmospheric modeling system to explore the following scientific questions: what is the relative role of the main processes between soil/vegetation and the atmosphere controlling the carbon cycle in *Amazônia*? What are the effects of biomass burning aerosols for each of these processes? What is the net

aerosol effect on the CO_2 fluxes? What is the relative effect of the direct interaction of aerosol radiation against the aerosol impact on the diffuse fraction? What is the regional dimension of the aerosol impact on CO_2 fluxes? Finally, how well can a state-of-the-art Chemical Transport Model (CTM) reproduce CO_2 fluxes and mixing ratio observations over the Amazon Basin?

5   The structure of this paper is as follows. In Sect. 2.1, we present a description of the most relevant aspects of the integrated atmospheric modeling system for this application. The adopted model configuration and the input data sets, including emissions and boundary conditions, are described in Sect. 2.2. The observational datasets, both from direct and remote sensing observation, used for model evaluation and analyses are described in Sect. 2.3. Model results are presented and discussed in Sect. 3. Sect 3.1 provides an overview of the meteorology and fire activity in *Amazônia* during the study period, including both

10 model results and observations. We then follow up in Sect. 3.2 with the model results for the regional biomass burning plume. Finally, in Sect. 3.3 we examine the model results for energy and CO_2 fluxes, related to several surface/atmosphere interaction processes, as well as the aerosol biomass burning impacts on them. The main results are summarized in Sect. 4.

2   Methods and data sets

2.1   Description of the relevant parts of the modeling system

15 In this work, we employed the integrated atmospheric-chemistry model BRAMS version 5.0 (Brazilian developments on the Regional Atmospheric Modeling System, Freitas et al., 2005, 2009, and 2016), which has been coupled in a two-way mode with the Joint UK Land Environment Simulator v3.0 (JULES), the land surface scheme of the UK Hadley Centre Earth System model, as described in Moreira et al. (2013). The coupling is two-way in the sense that, for each model time step, the atmospheric component provides to JULES the current near-surface wind speed, air temperature, pressure, condensed water

20 and downward radiation fluxes, as well as water vapor and carbon dioxide mixing ratios. After its processing, JULES advances its state variables over the time step and feeds back the atmospheric component with sensible and latent heat and momentum surface fluxes, upward shortwave and longwave radiation fluxes, and a set of trace gas fluxes.

Biosphere model: The Joint UK land simulator (JULES)

JULES simulates the exchange of carbon, momentum, and energy between the land surface and the atmosphere. Additionally,

25 it represents subsurface hydrological processes, plants photosynthesis and respiration, and vegetation and soil dynamics (Best et al., 2011; Clark et al., 2011).

    Atmospheric aerosols influence ecosystem functioning via effects on GPP from changes in quality and quantity of radiation but also indirectly via temperature effects on GPP but also on plant and heterotrophic respiration. The photosynthesis-radiation scheme, in JULES, accounts for the effects of diffuse radiation on canopy photosynthesis, by splitting direct and diffuse

30 radiation and sunlit and shaded leaves at each canopy layer. Specifically, the multilayer radiation scheme includes an explicit calculation of absorption and scattering of the direct beam and the diffuse radiation fluxes in both visible and near-infrared

wavebands, at each canopy layer, using the two-stream approach from Sellers (1985). Additionally, the attenuation of non-scattered incident direct beam radiation (sun flecks) is calculated using the approach by Dai et al. (2004). At each canopy layer, JULES estimates the fraction of absorbed direct and diffuse photosynthetic active radiation (PAR) thus providing a vertical profile of intercepted radiation fields which allows calculation of photosynthesis at each canopy level. At each canopy layer, the fraction of sunlit and shaded leaves is estimated as a function of the canopy beam radiation extinction coefficient (as explained in Clark et al 2011), and it is assumed that shaded leaves absorb only diffuse radiation and sunlit leaves absorb all types of radiation. Photosynthesis at each canopy layer is then estimated as the sum of sunlit and shaded leaf photosynthesis weighed by their respective fraction. Total canopy photosynthesis is estimated as the sum of the leaf –level fluxes in each layer scaled by leaf area of each canopy layer.

Temperature effects on photosynthesis are simulated in JULESs via biochemistry, leaf respiration and effects on vapor pressure deficit (VPD) on stomatal conductance in response to the temperature (see details in Clark et al. 2011). The temperature response of leaf respiration is linked to the temperature response of maximum carboxylation activity of Rubisco (Vcmax) in JULES, which is described by a peaked response function. The temperature response of remaining maintenance respiration components is simulated also using the leaf respiration temperature function. Growth respiration is estimated as a proportion of net primary productivity (NPP). Heterotrophic respiration is simulated either using a Q10 temperature function or a RothC temperature function (Jenkinson 1990 as described in Clark et al. 2011).

Evaluation of the skill of JULES in simulating GPP under high direct and high diffuse radiation conditions has been tested against flux sites in the Amazon and in temperate forest sites where direct and diffuse radiation measurements are available. This is shown in Figure 2 of Rap et al. (2015) at Tapajos and French Guyana in the Amazon and at two temperate forest sites in Mercado et al. (2009) (Figure 1). Investigation of the response of photosynthesis to changes in direct and diffuse radiation across relevant plant functional types for the Amazon region is carried out within this study.

Atmospheric model: Brazilian developments on the Regional Atmospheric Modeling System (BRAMS)

BRAMS is in-line coupled with a Eulerian transport model (CCATT) suitable to emission, simulate transport, dispersion, chemical transformation and removal processes associated with trace gases and aerosols (Longo et al., 2013). In CCATT, aerosol and trace gas transport runs consistently in-line with the atmospheric state evolution using the BRAMS dynamic and physical parameterizations. The tracer mass mixing ratio, which is a prognostic variable, includes the effects of sub-grid scale turbulence in the planetary boundary layer (PBL), convective transport by shallow and deep moist convection in addition to grid scale advection transport. For gaseous species, CCATT-BRAMS in principle can employ several gaseous chemical mechanisms. However, for this study, only carbon monoxide (CO), CO_2 and aerosol particles (biomass burning type) were emitted and transported. The physical removal processes (dry and wet deposition) were applied to all the three tracers, and effective lifetimes were applied to CO and aerosol particles. As the modeling of aerosol biomass burning particles is the focus of the present study, only biomass burning emission sources were considered.

The BRAMS model parameterizations chosen for the simulations performed in this work are described as follows. The parameterization for the unresolved turbulence in the PBL was based on the Mellor and Yamada (1982) formulation, which

predicts turbulent kinetic energy (TKE). For the microphysics, we used the single-moment bulk microphysics parameterization, which includes cloud water, rain, pristine ice, snow, aggregates, graupel and hail (Walko et al., 1995). It includes prognostic equations for the mixing ratios of rain and each ice category of total water and the concentration of pristine ice. Water vapor and cloud liquid mixing ratios are diagnosed from the prognostic variables using the saturation mixing ratio on liquid water. The deep and shallow cumulus convection schemes are based on the mass-flux approach and described in Grell and Freitas (2014).

The radiation scheme is a modified version of the Community Aerosol and Radiation Model for Atmosphere (CARMA, Toon et al., 1988), which includes the aerosol-radiation interaction with feedback to the model heating rates (Longo et al., 2013, Rosário et al., 2013). In addition, we included in CARMA a parameterization to calculate the diffuse fraction of solar irradiance specific for biomass burning aerosols in *Amazônia*. This parameterization was based on measurements of broad and narrowband solar global and diffuse irradiance components performed with a Multi-filter Rotating Shadow-band Radiometer (MFRSR – Harrison et al, 1994). With the narrowband measurements, centered at 415, 670, 870 and 1036 nm, AOD was estimated following the methodology of Harrison and Michalsky (1994) and Rosário et al. (2008). The measurements were performed at Reserva Biológica do Jaru, RO (-10.145°, -61.908°) during the dry/biomass burning season of 2007. The diffuse fraction of broadband irradiance reaching the surface as a function of AOD at 670 nm wavelength for distinct optical air mass intervals (m), expressed as a ratio of the optical path length relative to the path length at zenith, (Figure 1) was analyzed, and a three-degree polynomial fit was proposed as follows:

$$D = aAOD_{670}^3 + bAOD_{670}^2 + cAOD_{670} + d \tag{1}$$

D represents the diffuse fraction and the values of the fitting parameters a, b, c, and d, of the function in Equation 1 are described in Table 1. These fittings were achieved after filtering the data for clouds, which can be present even during the dry season, especially during days with low AOD values. When clouds are present, the diffuse fraction of radiation increases significantly with values as high as a very polluted atmosphere. However, as discussed below, the analysis presented here focuses only on areas, and during hours, without cloud cover, i.e. the results were obtained by filtering out the points with cloudiness, considering only the model gridboxes where the total column integrated condensed water was equal to zero. The aim of this work is only to compute the aerosol effect; therefore this filter was essentially used to exclude the effects of the clouds in the CO_2 fluxes.

2.2   Model configuration and input data sets

BRAMS model simulations were conducted for a domain covering the northern part of South America (southwest corner: 18° S, 90° W, northeast corner: 15° N, 30° W) using a regular grid with 20 km resolution, as illustrated in Figure 2. JULES was configured with 10 canopy layers. The chosen model domain encompasses the Legal Brazilian Amazon region (LBAR, depicted by the red line in Figure 2), which is a region of 5,016,136.3 km^2 (59% of the Brazilian territory). It hosts approximately 24 million inhabitants, which is only around 12% of the Brazilian population. The Brazilian Federal Law Nº 5.173 (Art. 2) established LBAR in 1966 as an administrative unit to promote sustainable development in one of the most, if not the most,

resource rich regions in Brazil. The main tropical biomes in South America, the Amazon rainforest, *Cerrado* and Pantanal (wetlands), are all found in LBAR. Despite government protection, deforestation activities, followed by vegetation fires, have led to extensive land use change to pasture and agricultural fields, and changes in atmospheric aerosol load and characteristics. This study aims to analyze the effect of these changes on the atmospheric environment, radiation budget, and forest productivity

5   in this important region.

The NCEP Global Forecast System analysis (http://rda.ucar.edu/datasets/ds083.2/), with 6-hourly time resolution and 1° × 1° spatial resolution, provided initial and boundary conditions for the time integration of the meteorological fields. Sea surface temperature (SST) was taken from NOAA Optimum Interpolation (OI) SST product, version 2, with 1° × 1° spatial resolution (available at http://www.esrl.noaa.gov/psd/data/gridded/data.noaa.oisst.v2.html, Reynolds et al., 2002). Data from

10 the RADAMBRASIL project (Rossato et al., 1998) was used for the soil type in Brazil and data from FAO (Zobler, 1999) was used outside Brazil. The model was run with seven soil levels: 0.10, 0.35, 1.0, 2.25, 4.25, 7.25 and 12.25 m below the surface. Soil moisture was initialized with the soil moisture estimation operational product developed by Gevaerd and Freitas (2006) and available at CPTEC/INPE, and the soil temperature was initialized assuming a vertically homogeneous field defined by the air temperature closest to the surface from the initial atmospheric data. The carbon data assimilation system,

15 Carbon Tracker 2015, (Krol et al., 2005; Peters et al., 2007), with 3° × 2° spatial resolution and 34 vertical levels, (available at http://www.esrl.noaa.gov/gmd/ccgg/carbontracker/), provided CO_2 initial and boundary conditions. Initial and boundary conditions for carbon monoxide (CO) were based on optimized fluxes, with 1° × 1° spatial resolution, as calculated by the 4D-var system using the Infrared Atmospheric Sounding Interferometer (IASI) data taken onboard the Eumetsat Polar System (EPS) Metop-A Satellite (Krol et al., 2013).

20 Biomass burning emissions of trace gases and aerosols were provided by the Brazilian Biomass Burning Emission Model (3BEM, Longo et al., 2010). The 3BEM emissions are based on a database of fire pixel counts and burned area derived from the combination of remote-sensing fire products from Geostationary Operational Environmental Satellite-Wildfire Automated Biomass Burning Algorithm (GOES WF-ABBA product; Prins et al., 1998), the Brazilian National Institute for Space Research (INPE) burning points observed, which is based on the Advanced Very High Resolution Radiometer (AVHRR) aboard the

25 NOAA polar orbiting satellites series (Setzer and Pereira, 1991), and the Moderate Resolution Imaging Spectroradiometer (MODIS) fire product (Giglio et al., 2003). Fire emissions were split into smoldering and flaming emission contributions, releasing trace gases and aerosol particles in the lowest model layer and in the injection layer, respectively, as determined by the in-line plume rise model (Freitas et al., 2007, 2010).

The land use dataset from the United States Geological Survey (USGS) at 1-km resolution was merged with a land cover

30 map for the Brazilian legal Amazon region (PROVEG) (Sestini et al., 2003). PROVEG is based on the Landsat Thematic Mapper (TM) images with spatial resolution of 90 m × 90 m from the year 2000 and deforestation data from the Amazon Deforestation Monitoring Program (PRODES) for the year 1997. At the 20-km resolution, each grid-box has 400 specifications of vegetation, which were reduced to 9 patches of different land cover categories (broadleaf trees, needle leaf trees, C3 and C4 grasses, shrubs, urban, inland water, soil and ice), each with its respective occupation fraction. JULES treats each category

35 separately and returns to BRAMS average fluxes weighted by the occupation fraction. The model results are then discussed for

the land cover categories present in the considered model domain: broadleaf trees (tropical forest), shrubs (*cerrado*), and C3 and C4 grasses (pasture). The land use map in the model domain is illustrated in Figure 2.

The model simulations were initialized on 15 August 2010 00:00 UTC and conducted for 45 days. We discarded the first 15 days as spin-up, and restricted our analysis to the month of September to avoid model artifacts related to the initial conditions.

5   A set of three experiments was performed. In the first one (hereafter named NO-AER), the aerosol-radiation interaction was neglected. The direct aerosol effect was taken into account in both the second (hereafter named DIR-AER) and third (hereafter named DIR+DIF) experiments, but only in the latter the diffuse fraction of radiation was passed to JULES. Otherwise it was set zero. Additionally, a long-term model run (2 years, from January 2010 to December 2011) was carried out only for the DIR+DIF model configuration.

10 **2.3   Method of analysis of the model results**

Comparing the carbon fluxes from the three model simulations should allow us to assess the aerosol effect on CO_2 uptake in *Amazônia* and the relative roles of surface temperature, the direct aerosol effect and the increase in the diffuse fraction of PAR due to aerosol scattering. The CO_2 fluxes from the model were analyzed as the variation related to the total aerosol effect (both on diffuse radiation and direct radiation):

$$\Delta Flux_{tot} = Flux_{DIR+DIF} - Flux_{NO-AER} \tag{2}$$

Only with the direct radiation aerosol effect:

$$\Delta Flux_{dir} = Flux_{DIR-AER} - Flux_{NO-AER} \tag{3}$$

And, only with the diffuse radiation aerosol effect:

$$\Delta Flux_{diff} = Flux_{DIR+DIF} - Flux_{DIR-AER} \tag{4}$$

20 We examined the spatial distribution and diurnal cycles of CO_2 fluxes, related to several surface/atmosphere interaction processes. In addition GPP, we also looked at the CO_2 fluxes associated with plant respiration (R_P), soil heterotrophic respiration (R_P,), and the net ecosystem exchange ($NEE = R_P + R_H - GPP$), which is a measurement of the quantity of carbon entering and leaving the ecosystem (negative when the ecosystem is a CO_2 sink, and positive when is a CO_2 source). The spatial distributions of CO_2 fluxes are presented as monthly mean in $\mu molC\,m^{-2}\,s^{-1}$ for September 2010 at 1600 UTC, which is around noon local time for most of *Amazônia*. The diurnal cycles of CO_2 fluxes are presented as hourly monthly means in units of $\mu molC\,m^{-2}\,s^{-1}$ for September 2010, considering the model grid-cells circumscribed in the LBAR region delimited in Figure 2. The monthly net values of CO_2 fluxes in the LBAR are calculated as the integral of the mean diurnal cycles, and presented in $TgCmonth^{-1}$, considering the LBAR area of $\sim 5.2\,10^{12}\,m^2$, which is the total area of the model cells circumscribed in the LBAR region delimited in the Figure 2, multiplied by 30 to get the monthly total.

30 Because each biome has its own characteristics and responds differently to changes occurring at or under the surface and in the atmosphere, we first examined how each biome responds to the presence of biomass burning aerosol, both in terms of total

irradiance attenuation near surface and increase of the diffuse fraction of PAR. We also evaluated the relative contribution of the diffuse to the total (diffuse + direct) aerosol effect on the CO_2 fluxes for each the biome type. After assessing the specific behavior of each biome, model results for CO_2 and energy fluxes from each biome were then averaged, weighting by the biome fraction of each grid, to address the heterogeneity of the Amazon region in terms of land cover and local climates.

5   ## 2.4   Data sets for model evaluation

The model results for precipitation and near-surface temperature were contrasted with direct observations and products derived from satellite observations. The aerosol biomass burning spatial distribution from the model was validated with remote sensing products. Additionally, model performance on simulating CO and CO_2 mixing ratios was assessed using measurements of carbon monoxide (CO) and CO_2 concentration in air samples collected over the Amazon during 2010 and 2011. The CO

10   concentration varies as a function of fire source, horizontal and vertical transport and deposition. It was not coupled with the biosphere model. Therefore, the DIR-AER and DIR+DIF scenarios have similar concentration distributions.

Biomass burning mainly releases water vapor and CO_2 to the atmosphere but is also a major source of other tracers, such as CO, volatile organic compounds, nitrogen oxides, and organic halogen compounds (Andreae and Merlet, 2001). An enhancement of CO has been historically observed in *Amazônia* during the dry season, which is mostly attributed to fire emissions, because volatile organic compounds (VOC) oxidation is expected to have little seasonality in *Amazônia* (Holloway et al., 2000;

15   Duncan and Logan, 2008, Andreae et al., 2012). Therefore, the evaluation of CO mixing ratios from the model against observations provides an assessment of model skill to simulate fire emissions, its transport, and removal. We also looked into fire activity and used the soil moisture and meteorological variables from the model as indicators of spatial scale of locations where fires were more likely to occur. The datasets used for model evaluation are described below.

20

Precipitation: Monthly mean precipitation over the Amazon region was obtained from the algorithm 3B42 of the Tropical Rainfall Measuring Mission (TRMM) merged high quality (HQ)/infrared (IR) precipitation product at a spatial resolution of $0.25° \times 0.25°$ (http://trmm.gsfc.nasa.gov/3b42.html; Kummerow et al., 1998; Kawanishi et al., 2000). TRMM 3B42 is derived from retrievals of 3-hourly precipitation amount from the precipitation radar (PR), TRMM microwave imager (TMI),

25   and visible and infrared scanner (VIRS) aboard the TRMM satellite, merged with rain gauge data from the Climate Anomaly Monitoring System (CAMS) and the Global Precipitation Climatology Project (GPCP). Satellite estimates of precipitation were used for model evaluation due to their more complete spatial and temporal coverage compared to rain gauge data. The latter was also complementarily used to evaluate modelled precipitation and temperature, though not ignoring the low density and heterogeneous distribution of the observational network in the geographical model domain: 72 PCDs (automatic stations

30   installed and maintained by the Brazilian National Institute of Meteorology - INMET) in 5,016,136.3 km^2.

Temperature: We evaluated the mean diurnal cycle of 2-meter temperature from the model with data from 72 near-surface measurement ground stations in the LBAR, locations depicted in Figure 3.a.

Fire activity: We checked the coherence of soil moisture results from the model with the burning points observed from Advanced Very High Resolution Radiometer (AVHRR) onboard the NOAA polar orbiting satellites series. The fire detection used is based on the AVHRR retrieval algorithm from the Brazilian National Institute for Space Research (www.cptec.inpe.br/queimadas).

5

Biomass burning CO and CO$_2$: Model performance in simulating CO and CO$_2$ mixing ratios was assessed using measurements of carbon monoxide (CO) and CO$_2$ mole fraction ("concentration") in air samples collected over the Amazon during 2010 and 2011. The air samples were collected with portable sampling systems consisting of separate compressor and flask units (Tans et al., 1996) onboard a Cessna 206 aircraft in descending spirals from 4,300 to 300 m over four Amazon

10   locations indicated in Figure 2: *Santarém*, PA (2.43° S, 54.72° W), *Rio Branco*, AC (9.97° S, 67.81° W), *Alta Floresta*, MT (12.54° S, 55.71° W), and *Tabatinga*, AM (4.25° S, 69.94° W). The air samples collected in *Santarém*, *Rio Branco* and *Alta Floresta* are characteristic of the moist tropical forest, both primary and secondary, surrounding them. During the dry season, both local (forest), and remote *cerrado* and pasture fire emissions affect these three sites. The samples collected in *Tabatinga*, which is further west, in a more pristine area of the Amazon forest, respond to the influence of the intact forest landscape

15   upwind. During the dry season, fire emissions influence the atmospheric chemistry in all sites, although the biomass burning impact in *Tabatinga* is more related to episodic long-range transport events, and so not as persistent as the others. The air sampling was always between 12:00 and 14:00 local time and analyzed at the laboratory of the *Instituto de Pesquisas Energéticas e Nucleares* (IPEN) in *São Paulo*, Brazil. Measurements precision of CO$_2$ and CO is estimated to be around 0.04 ppmv and 0.5 ppbv, respectively. For further details, regarding air sampling and analytical methods, see Gatti et al. (2010).

20   We also used CO$_2$ measurements in the *Tapajós* National Forest near km 67 (02.85°S, 55.04°W) of the *Santarém* – Cuiabá highway, just south of *Santarém*, for model evaluation. The *Tapajós* measurements are based on eddy covariance methods, using the profile mixing ratio data to estimate the change in vertical average mixing ratio between the ground and flux measurement height to calculate the column average storage of CO$_2$ (Saleska et al., 2003). CO$_2$ mole fractions were measured at 8 levels along the tower (62.2, 50, 39.4, 28.7, 19.6, 10.4, and 0.91 m). Sample air was drawn and analyzed with an infrared

25   gas analyzer (IRGA, LI-6262, Licor, Lincoln, NE). Pressure and temperature of the Licor cells are controlled. The IRGA was automatically zeroed every 2 hours and the Licor profile, every 20 minutes. All Licors are automatically calibrated with span gases every 6 hours.

Biomass burning aerosol: The AOD (Aerosol Optical Depth) product derived from MODIS sensors onboard of the Aqua

30   satellite is used to evaluate the simulated biomass burning aerosol plume. In this work, we used the MODIS Level 2.0 Collection 5.1 (051) data and Level 3 Atmospheric product denominated MYD08_D3 (Mean Aerosol Optical Thickness at 550 nm).

3 Model results and discussion

3.1 Meteorology, fire activity and regional biomass burning plume

Temperature: The simulated 2-meter temperature in the central portion of the Amazon Basin during September 2010 peaked around 32 °C at 1600 UTC, while the northwest region was slightly cooler, typically ranging from 30 to 28 °C (Figure 3.a).
Going southeast, towards the *cerrado* region, the mean 2-meter temperature reached 35 °C at 1600 UTC. The temperature gradient is mostly associated with the gradient of soil moisture and land cover in the region. The evaluation of the mean diurnal cycle of 2-meter temperature from the model against observations using 72 near-surface measurement ground stations in the LBAR during the same period shows that the model results are consistent with observations (Figure 3.b), though the model mean temperature was typically cooler (∼2.5 °C) during the night period and late afternoon hours, and was not far from the standard deviation of the observed mean temperature. In addition, the model temperature has a diurnal cycle with a gap of one hour more early than the observation.

Precipitation: The monthly mean rainfall data from the ground stations monitoring network, interpolated to the model grid points (Figure 4.a), and the TRMM rainfall product (Figure 4.b), both reveal a well-defined spatial distribution of the precipitation in the northern region of South America during September 2010. First, in the southeast Amazon, accumulated rainfall was low, with values typically lower than 50 mm for this month; the northwestern region was wetter, with accumulated values around 200 mm. In addition, there were few areas of high rainfall in the northern part of South America, mainly in the Guiana Highlands, associated with the topographic forcing. The general spatial distribution of model accumulated precipitation (Figure 4.c) compares well with ground observations (Figure 4.a), with an indication that the model overestimated the total precipitation. However, one must take into account that the measurement stations are very scarce in this region, making detailed comparisons difficult. Interpolation in the presence of limited information usually reduces the intensity of precipitation, spreading the value observed around the neighboring grid points without data available. Indeed, the precipitation estimated by TRMM (Figure 4.b) agrees much better with the model results (Figure 4.c).

Soil moisture and fire activity: As a result of the precipitation distribution, the soils are predominantly wetter in the northwestern part of South America, with simulated volumetric moist content ranging from 0.35 to 0.45 $\mathrm{m^3m^{-3}}$ for all soil layers (Figure 5). The high soil moisture of the northwestern *Amazônia* contrasts with the rest of the region's dryness, where the moisture in the top soil layer of the model is below 0.2 $\mathrm{m^3m^{-3}}$ (Figure 5.a), and only deeper soil layers remain fairly moist (0.3 $\mathrm{m^3m^{-3}}$, below 4 m) (Figure 5.c). Comparing soil moisture in two forest areas with different rainfall regimes (red rectangle, 148 mm in average) and blue rectangle (34 mm in average), the area receiving a higher volume of rainfall is about 55% wetter than the other in the shallow layers, but only 12% in the deeper soil layer. By contrast, comparing areas of forest (blue rectangle) and *cerrado* (gray rectangle) with similar rainfall regime (34 mm), the forest region remains considerably wetter (15% both in shallow and deeper layers). According to Köchy & Wilson (2000), high rates of water uptake per unit mass may reflect the high root density of the vegetation. In fact, James et al. (2003) found at a site 20 km east of Regina (58°28'N,

11

104°22'W), Canada, that the ability of grass to reduce soil moisture is nearly five times higher than that of woody vegetation, expressed on a per-gram basis. For the forest region, the soil moisture values from the model are consistent with the mean value of 0.39 m^3m^{-3} measured at 0.2 m at *Tapajós* site (near *Santarém*, location indicated in Figure 2) during the dry season (Doughty et al., 2010). Previous measurements at the same site, reported soil moisture only slightly higher at the same site

5 (0.44 m^3m^{-3} , from 0.15 to 0.30 m), and also confirmed the model results for a higher moisture of the deeper soil layers (0.42 m^3m^{-3} at 4 m) (Bruno et al., 2006).

The period chosen for this study coincided with the peak of the biomass burning season when a total of 439,297 fires were detected in the area of the model domain by AVHRR-NOAA, which is 42% of the total number of fires detected by the same sensor during the entire burning season. The spatial distribution of the fires resembles the pattern of precipitation and soil

10 moisture simulated by the model (Figure 5). Nonetheless, most of the fires were ignited by human activities (Nepstad et al., 1999; Cochrane & Laurance, 2008). Fires occurred mostly in the *Cerrado*, C3, and C4 type grass-covered areas, but forest fires, with much higher biomass density, are typically responsible for the highest amount of biomass burning aerosols and trace gases released into the atmosphere. Figure 6 depicts the spatial distribution of vegetation fires detected by remote sensing over the Amazon and Central Brazil during September 2010.

15

Smoke regional plume, CO and CO_2 mixing ratios: Model results for CO mixing ratio as simulated by the DIR+DIF experiment, which are expected to be the most realistic, were compared with CO vertical profile measurements from four different sites in *Amazônia*. The time series of CO mixing ratio, derived from observations, and model results around 2 km above ground level in four different locations in *Amazônia* (*Alta Floresta*, *Santarém*, *Rio Branco*, and *Tabatinga*) are shown in

20 Figure 7 (top - left). There was an enhancement of CO from July to October for both years in all the four locations. In 2010, the CO mixing ratio values in the PBL during the dry season increased from 100 - 150 ppb, typical wet season values (Andreae et al., 2012), to up to 500 ppb, both in the simulations and observations. The dry season of 2010 had CO mixing ratios about twice higher than the same period in 2011, which is consistent with the total number of fires detected by remote sensing during the dry season of these two years which approximately doubled (http://www.inpe.br/queimadas/estatisticas.php). Scatterplots

25 of the CO mixing ratio values from observation and model results for the same four locations, separated into several vertical layers, are depicted in Figure 7 (top – right). The CO background mixing ratio values for the *Tabatinga* site are close to the 1:1 line, while the biomass burning affected values are more scattered. Model results show good agreement with observations but tend to underestimate CO and CO_2 observations, especially at low levels, in locations mainly affected by fire emissions both locally (*Alta Floresta*, *Rio Branco* and *Santarém*) and by long range transport (*Tabatinga*). The black line on each scatter plot

30 in Figure 7, shows the linear fit and the correspondent R-Squared values. The largest underestimation of CO occurred in *Alta Floresta*, with a slope of 0.58, but the biggest dispersion occurred in *Santarém*, with $R^2 = 0.58$. This pattern is probably related both to the 20-km model resolution not picking up individual biomass burning plumes and fire emissions underestimation (Pereira et al., 2016). Previous studies indicated that biomass burning emissions contribute more than 95% to the variability of CO over the Amazon and that the emissions used in this study (3BEM, Longo et al., 2010) are about 20% underestimated

35 (Andreae et al., 2012).

On the other hand, the airborne vertical profiles analyzed in this study and our modeling results indicated a lesser enhancement of CO_2 related to fire activity compared to CO. These results are in agreement with previous measurements of fire biomass burning plumes that showed relatively small enhancements of CO_2 relative to the background in *Amazônia* and indicated that fire emissions were expected to contribute only minorly to CO_2 mixing ratios in *Amazônia* (Andreae et al., 2012). Figure 7

5   (bottom – left) shows the observed –airborne air sampling at around 2 km above ground level –and simulated time series of CO_2 mixing ratios. The major uncertainty of the CO_2 mixing ratios is probably most strongly related to the vertical transport and fresh smoke plumes and uncertainty in the forest NEE. For example, the misplacement of convective systems of few grid cells, very acceptable for a low-resolution atmospheric model, can produce huge variations in the CO_2 values near the surface. In addition, the timing of the convection in tropical region is a well known limitation of atmospheric models in general.

10 Nonetheless, the CO_2 scatter plots (Figure 7, bottom - right) evidenced a much higher variability of both observed and modeled values compared to CO, as well as a poorer model representation values close to the ground compared to the upper levels. The low-level behavior is likely to be associated with local convective processes but could also have a minor contribution from fresh biomass burning plumes, both venting CO_2 and changing locally the diffuse fraction of solar radiation. By contrast, the model tends to better represent the upper levels in terms of observed CO_2, which is due to the fact that air circulation is more

15 intense and mainly controlled by the Carbon Tracker boundary conditions, and fire emissions contribution becomes even less significant. However, the model is not sensitive to the CO_2 concentration within the given range, and therefore the model problems reproducing point observations should not have a major effect on the final results.

biomass burning regional plume – AOD: In Figure 8, we show the mean regional biomass burning plume for September

20 2010 through the monthly mean of AOD at 550 nm wavelength both from MODIS-Aqua retrieval (Figure 8.a) and from the DIR+DIF model simulation (Figure 8.b). A substantial portion of central Brazil and neighboring countries and the southern Amazon Basin were covered by smoke with a resulting monthly mean AOD higher than 0.5, which is 3 to 5 times larger than the typical values of clean conditions. Moreover, there were also large sub-areas with monthly mean AOD higher than 1, indicating a persistent and high loading of smoke particles. The model results fairly reproduced the spatial distribution of the

25 regional smoke plume from MODIS retrievals. A scatter plot of AOD values from the model and MODIS retrieval (Figure S.5 in supplementary material) presents a slope of 0.71 (with $R^2 = 0.73$). Conversely, MODIS retrievals tend to overestimate AOD in relation to the AERONET retrievals in *Amazônia*, especially for high aerosol loadings (Hoelzemann et al., 2009). Analysis of model results versus AERONET retrieval in some sites in the southern *Amazônia* (not shown), confirmed that the order of magnitude of the model underestimation is about the same 20% previously estimated.

30

Site level –plant atmosphere CO_2 exchange: Figure 9.a shows the mean diurnal cycle of CO_2 mixing ratio in the first model layer of the three experiments together with the mean diurnal cycle of CO_2 mixing ratio just above the canopy of the *Tapajós* forest (near *Santarém*, location indicated in Figure 2) from measurements during September 2010. In *Tapajós*, both observation and model results present a nighttime increase of CO_2 due to plant respiration, peaking shortly after sunrise, and

35 a daytime decrease due to photosynthetic processes, with the lowest values before sunset. Despite the model difficulties in

simulating the CO_2 mixing ratio near surface, on average, the discrepancies with observation were only about 0.9% and 1.4% for the maximum and minimum values, respectively, with the model values lower than the observation during the peak hour and vice-versa when the photosynthetic process dominates. The model amplitude of the CO_2 cycle is lower than that observed, though the model cycle is still within the standard deviation of the mean observed diurnal cycle. Model results without including aerosol effects (NO-AER) and with the inclusion of the direct aerosol effect only (DIR-AER) produce a very similar CO_2 diurnal cycle. However, the inclusion of the diffuse radiation effects due to biomass burning aerosols reduces the values of CO_2 mixing ratio and brings model results much closer to observation, especially during the day, even though the mean AOD modeled in *Tapajós* was very low compared to the area mostly affected by biomass burning and even underestimated by the model. A curious fact is that at night the difference between NO-AER and DIR+DIF is greater than in the daytime period. One possible explanation for this is the influence of the neighborhood. Note in Figure S.6 of the supplementary material that the average wind at 00 UTC is from east, a forest region, and has differences between aerosol and non-aerosol simulations. However, the wind at 10 UTC is coming from northeast, crossing the river, where the influence of the aerosol in the carbon fluxes is low. Considering the whole LBAR area, which includes the region with the highest aerosol load, the inclusion of the aerosol effect on CO_2, especially the effect of the diffuse radiation, reduced the CO_2 mixing ratio of about 10 ppmv in the CO_2 mixing ratio all day long (Figure 9.b). The shift of the diurnal cycle of CO_2 mixing ratio from the model relative to the observation in *Tapajós* is likely to be related to the AOD underestimation.

In the next section, we will present the model results for energy and carbon fluxes and explore the role played by the biomass burning aerosol in the carbon cycle in *Amazônia*.

3.2 JULES sensitivity test

We performed sensitivity tests to assess JULES response to several atmospheric variables. We ran JULES offline (version 3.0) for September 2010 using as input BRAMS results for the NO-AER experiment considering the nearest gridbox to the Tower km-67. Figure S.1 (in the supplementary material) shows monthly variation of downwelling shortwave (Rshort) and longwave irradiance (Rlong), air temperature near surface and specific humidity near surface, all used as input for the sensitivity test. The soil carbon in this gridcell is 10 kgCm^{-2} during the all month. Besides using the BRAMS model results for each parameter, we also varied each parameter, reducing and increasing its original value to cover the standard deviation of the monthly mean. In addition, we varied the diffuse fraction of the shortwave radiation, which was originally zero (NO-AER scenery), from 0 to 0.8 of the total radiation. Therefore, we ran 567 simulations for the month of September 2010. For each simulation, we calculated the monthly mean fluxes. Figures S.2, S.3 and S.4 show the results for these sensitivity tests. JULES results for soil respiration, and consequently NEE, are quite sensitive to the prescribed soil carbon content (Figure S.2). In addition, the GPP increases with the increase of soil moisture for all biomes (Figure S.3). However, R_H and R_P also increases with the soil moisture (Figure S.3a and S.3m). Therefore, for the forest and *cerrado* biomes, the NEE decreases until a certain value, after then increases again with the increasing of soil moisture (Figure S.3s). In summary, the sensitivity analyses show that i) for a 7% decrease in shortwave radiation there are minimal changes in GPP (Figure S.4a); ii) a change in temperature of one degree Celsius (from current midday conditions) also did not imply in major changes in the simulated GPP (Figure S.4b); and

iii) a 40% increase in the diffuse fraction of shortwave radiation increased the GPP by 39% , 71%, 4%, and 72% in forest, C3, C4 grasses, and *cerrado* (shrubs) vegetation , respectively (Fig S.4c).

3.3   Impacts of biomass burning aerosol on energy and carbon fluxes

Incoming Radiation: The modeled mean downwelling shortwave irradiance at surface (RSHORT) at 1600 UTC during September 2010 from DIR-AER experiment ranged from 900 Wm^{-2}, in the southwestern Amazon, to 1000 Wm^{-2} in the northeastern portion (Figure 10.a), with the biomass burning aerosol direct impact ($\Delta RSHORT = RSHORT_{DIR-AER} - RSHORT_{NO-AER}$) reaching -100 Wm^{-2} in biomass burning areas (AOD > 0.5) (Figure 10.b). As a consequence of the biomass burning aerosol direct effect, the 2-meter temperature decreased by 1.2 °C in average in the biomass burning areas around midday ($\Delta Temp = Temp_{DIR-AER} - Temp_{NO-AER}$, Figure 10.c). The noise in the northwestern region for both RSHORT and temperature differences within the two simulations is related to expected nonlinear aerosol perturbations on cloud distribution. These results are consistent with previous modeling studies (Rosário et al., 2013) and with estimations based on AERONET measurements (Procópio et al., 2004). Additionally, observations in *Tapajós* during the dry season indicate an average reduction of 80 and 123 Wm^{-2},for $AOD > 0.5$ and $AOD > 0.7$, which corresponded to a decrease of the mean temperature of 0.26 and 0.41°C, respectively.

The presence of biomass burning aerosol in the atmosphere also impacts the flux of PAR in *Amazônia* during the dry season. Monthly mean PAR ($\mu\mathrm{mol\ m}^{-2}\ \mathrm{s}^{-1}$) at 1600 UTC, which is around midday in most of *Amazônia*, as simulated by the DIR+DIF model experiment for September 2010 is depicted in Figure 11.a. The modeled PAR monthly mean values at 1600 UTC ranged between 900 - 1000 $\mu\mathrm{mol\ m}^{-2}\ \mathrm{s}^{-1}$ from southwest to northeast in the LBAR. The presence of biomass burning aerosol increases the diffuse fraction of radiation by up to 40% in the biomass burning areas (Figure 11.b). Figure 12.a shows the diffuse PAR as a function of AOD.

Decreases in surface temperature due to the direct effect of aerosol are also influenced by the balance between latent and sensible heat fluxes, or ultimately, on soil moisture. The difference in 2-meter temperature ($\Delta Temp$) and shortwave irradiance ($\Delta RSHORT$) is, as expected, highly correlated, though with a large band of $\Delta Temp$ for the same value of $\Delta RSHORT$ (Figure 12.b). The $\Delta Temp$ bandwidth increases almost linearly with the $\Delta RSHORT$, with the values correspondent to higher soil moisture populating the lower part of the curve (Figure 12.b), meaning that for regions with the same AOD, the ones with drier soil will suffer higher surface cooling.

Carbon fluxes for the vegetation types in *Amazônia*: Spatial fields for simulated GPP across the northern part of South America are presented in Figure 13.a for September 2010 at 1600 UTC for forest, C3G, C4G, and shrub in rows 1 -4, respectively. Over forest, simulated GPP ranges from 20 to 25 $\mu\mathrm{molC\ m}^{-2}\ \mathrm{s}^{-1}$; while over the regions occupied by *cerrado*, pastures, and tinges of forest there was a much higher variability, with GPP widely varying from below 5 to above 20 $\mu\mathrm{molC\ m}^{-2}\ \mathrm{s}^{-1}$. In Column b of the Figure 13 we show the difference between monthly mean GPP as simulated for the DIR+DIF and NO-AER experiments, i.e. the relative impact of the total effect of aerosols on simulated GPP for the 4 studied biome types: forest (b.1), C3G (b.2), C4G (b.3) and *cerrado*(b.4). In column c, we show the difference between monthly mean

GPP of the simulation without the aerosol effect on the diffuse radiation (DIR-AER) and the simulation without any aerosol effects (NO-AER), i.e. we evaluate the relative impact on the direct solar radiation effect.

In Figure 14.a, one can note that the mean solar irradiance that reaches the Amazon region during September promotes a high GPP for the C4 plants even into the local afternoon when C3 plants close their stomata to reduce water loss. Thus, typically, the GPP of the C4 type plants are highly correlated with the amount of irradiance received. Therefore their GPP resembles the same diurnal cycle shape of the irradiance. By contrast, the other vegetation types suffer, in a less or more extent, a decrease in the carbon assimilation during the period of maximum irradiance, therefore reshaping their GPP diurnal cycle. Still in Figure 14.a, the net increase in GPP due to biomass burning aerosol over forest (ΔGPP_{tot}, difference between the curves in red and green filled squares) is 3.8 µmolC m^{-2} s^{-1}, with the majority ($\%Flux_{diff} \cong 94\%$) of the impact related to the increase in the diffuse fraction of solar radiation. The reduction of direct solar radiation by biomass burning aerosols increases forest GPP only up to 0.2 µmolC m^{-2} s^{-1} (ΔGPP_{dir}), which is associated with the cooling of the leaves. Over *cerrado* areas, the increase on GPP was up to 0.9 and 0.1 µmolC m^{-2} s^{-1} due to the aerosol effect on the diffuse fraction radiation (ΔGPP_{diff}), and the direct radiation (ΔGPP_{dir}), respectively, with the aerosol direct radiative effect much lower than the diffuse radiation effect because the GPP of the *cerrado* is also severely limited by the excess of irradiance. In the case of the C4 grass type, which was not limited by irradiance, the direct radiative aerosol effect induced a reduction of the GPP (-0.7 µmolC m^{-2} s^{-1}), but the increase in the diffuse fraction of radiation more than compensate the reduction of GPP due the irradiance attenuation of the direct effect, and, when including both direct and diffuse radiation effects, the GPP increases from 43 µmolC m^{-2} s^{-1} to 47 µmolC m^{-2} s^{-1}. Table 2 summarizes the integrated values of GPP for each biome in the LBAR during September 2010, as well as the variation related to the total aerosol effect (both on diffuse radiation and direct radiation, ΔGPP_{tot}), and only with the direct aerosol effect (ΔGPP_{dir}). According to the model results, the net GPP of the forest biome in the LBAR was of 1,206 Tg C during September 2010. The presence of biomass burning aerosol was responsible for an increase of about 32% of the GPP over the forest, mainly associated with the impact of the aerosol on the diffuse radiation. For the *cerrado* and C3 grass, the net GPP was 359 and 850 Tg C in the same region, during the same period, with the biomass burning aerosol acting to increase the GPP of about 20% and 30%, respectively. We estimated an average increase of 27% in GPP for September 2010 in the LBAR region, associated to the aerosol effect in *Amazônia* (Table 4). However, Rap et al. (2015), using JULES model forced with aerosol field from another model, estimated an average increase in GPP of only 2.8% for August, considering the period of 1998-2007. Also, our estimate of net primary production ($NPP = GPP - R_P$) for the DIR+DIF simulation was 553 TgC/month (1,113 - 560) and 363 TgC/month ((1,113-240)-(560-50)) for NO-AER. Therefore, we estimate an increase of 52% in NPP for September 2010, due the aerosol in LBAR region, while Rap et al. (2015) estimated a increase in NPP of only 5.4% for August. Our results for the aerosol impact over the *Amazônia* is higher than the Rap et al. (2015) estimation. However, one must keep in mind that Rap et al. estimation was based on 9 years (1998 – 2007) and for a month (August) that typically has much lower aerosol loading than September, while our work was based on September, the peak for the biomass burning season, and for 2010, a drier and smokier year. The diurnal cycle of plant respiration for each biome is shown in Figure 14.b for the three model runs. As expected, higher GPP leads to higher plant respiration. Plant respiration peaks 7.5, 2, 4.6, and 14 µmolC m^{-2} s^{-1} for forest, *cerrado*, C3, and

C4 grass types, respectively, with the aerosol impact more pronounced for forest and C4 biomes. The mean soil respiration found in the LBAR is 2.78 μmolC m^{-2} s^{-1}, with a relatively mild diurnal cycle that basically depends on soil temperature, hence with lower values in the morning and a tendency to increase slightly in the afternoon. However, soil respiration is highly variable in the LBAR, depending on the amount of carbon in the soil, being as low as 0.13 μmolC m^{-2} s^{-1} in the *cerrado*

5 and grass-plot areas, and ranging between 2 and 8 μmolC m^{-2} s^{-1} in forest areas. Regarding NEE, model results show that the forest biome released around +5 μmolC m^{-2} s^{-1} during the night and early morning, and then, when GPP compensates the respiration, the net uptake goes as low as -11 μmolC m^{-2} s^{-1}. The net effect is an uptake of approximately 0.015, 0.565, and 0.060 molC m^{-2} day^{-1} for the C3, C4 grass, and forest biomes, respectively, and a release of 0.126 molC m^{-2} day^{-1} for the *cerrado*. Grace et al., (1995), with measurements of CO$_2$ fluxes at Jaru Reserve, Rondônia, Brazil (10°,4.84'S, 61°,

10 56.60'W) in September 1992, estimated an accumulation of 0.09 molC m^{-2} day^{-1} for forest during the dry season. So, the forest uptake estimation based on our modeling results is approximately 30% lower than the estimations based on Grace et al. (1995) measurements. However, several measurements in the Amazon indicated both high yearly and regional variabilities around the Amazon Basin due to several factors, which include hydric stress, aerosol loads, topography, differences in soil carbon and forest physiology. Also, previous studies indicated that there are high uncertainties in the magnitude of nocturnal

15 NEE measurements because of the lack of turbulence in and above the forest (Araujo et al., 2002; Araujo et al., 2010). In Table 3 we collected from the literature some estimates of NEE (daily total, nighttime and daytime peak), based on CO$_2$ fluxes measurements in different sites in *Amazônia* during the dry season in different years. For the same sites, we also presented in Table 3, the NEE from DIR+DIF experiment for September 2010. For example, measurements taken at the Jaru reserve (the same site used by Grace et al., 1995) and at a grass-plot (Fazenda Nossa Senhora - FNS, at 10°45'44"S, 62°21'27"W), during

20 the dry season from 1999 to 2002, revealed an uptake of around 0.12 and 0.069 molC m^{-2} day^{-1} for the pasture and forest site, respectively, with the diurnal values of NEE reaching -13.2 and -17.5 μmolC m^{-2} s^{-1} for the pasture and forest, respectively (von Randow, 2004). And, more recently, Cirino et al. (2014) reported 10 years of CO$_2$ fluxes measurements carried out in central Amazon's Cuieiras Biological Reserve – K34 LBA (Large Scale Biosphere-Atmosphere Experiment in *Amazônia*) tower flux (2°36'33" S, 6°12'33" W) from 1999 to 2009, and also in the Jaru reserve from 1999 to 2002. The measured diurnal

25 cycle of NEE at both sites was, as expected, positive during the night time and negative during the daytime. During the dry season, the mean values of NEE measured during the night were approximately +5.2(±0.8) and +6.8 (±1.0) μmolC m^{-2} s^{-1} at the Jaru (Von Randow et al., 2004) and Cuieras (Cirino et al., 2015) reserves, respectively, due to differences in the physiology of the forest, and possibly topography in the two sites. There were even more significant differences between the maximum values of carbon uptake between the two sites, which were around -17.5 and -20 μmolC m^{-2} s^{-1} under biomass burning and

30 cloudy sky condition, at the Jaru and Cuieras reserve, respectively, and -18 μmolC m^{-2} s^{-1}, under clean-sky in both sites. The differences between the peak values of carbon absorption are likely related to the presence of biomass burning, variability of cloudiness and rainfall, and soil characteristics, like water content, nutrients (N, P), etc.. Measurements at the *Tapajós* National Forest (2°51'S,54°58'W) from 2002 to 2005 (during September) led to estimations of NEE varying from +0.017 to –0,069 molC m^{-2} day^{-1} (Hutyra et al., 2007). The mean value of NEE from the model at *Tapajós* was -0.032 molC m^{-2} day^{-1}

35 for September 2010. The Jaru reserve is systematically, intensely affected by both local and long range transported biomass

17

burning aerosols, with monthly means for AOD (550 nm) during the dry season typically above 0.5, but often above 1.0; in contrast, the biomass burning affects the northern part of the Basin, where Cuieras and *Tapajós* are located, more episodically (Longo et al., 2009). In addition, the northern part has more variability in terms of rainfall during the dry season compared to the southern part, due mainly to the position of the Inter-Tropical Convergence Zone (ITCZ). So, a strong variability in the

5   terms of carbon fluxes in the northern part of the Amazon is indeed expected and is really challenging for a low-resolution model to match point measurements. Nevertheless, our modeled monthly mean diurnal cycles of NEE for forest and pasture biomes (Figure 14.c) are remarkably close to the diurnal cycle reported for the Jaru reserve and FNS, respectively, by von Randow et al., (2004), with the total daily total, nighttime, and daytime peak values (Table 3) of similar order of magnitude within the variability observed.

10 Figure 15 depicts the model results of DIR+DIF simulation for GPP (μmolC m^{-2} s^{-1}) in response to the available PAR (μmol m^{-2} s^{-1}) for the main four different biome types in the domain of study and in a range of 0.2 to 0.6 of the fraction of the diffuse irradiance. The analysis is also limited to the condition where the soil wetness is above 0.9. The maximum values of GPP for Forest and C3 type grass are reached with PAR around 1,600 mol m^{-2} s^{-1} and 1,300 mol m^{-2} s^{-1}, respectively, indicating that these are the saturation point for these biomes relative to the amount of energy reaching the surface. For *cerrado*

15 (shrub), the saturation point is much lower, around 600 mol m^{-2} s^{-1}, but the plants maintain its carbon assimilation rate up to PAR around 1,600 mol m^{-2} s^{-1}, only then decreasing with further increase of PAR. For the C4 type grass, GPP increases almost linearly with PAR, not showing any evidence of saturation with the amount of energy received. In general, the results in Figure 15 indicate that, for a given biome and amount of PAR, higher amount of the diffuse radiation implies higher GPP. However, the *cerrado* (shrub) biome is an exception since it saturates with relatively lower values of PAR.

20 The mean spatial distribution of the relative impact of aerosol effects on modeled fluxes at 1600 UTC is shown in Figure 16 considering the changes both on direct and diffuse radiation, and only on direct solar radiation. In the LBAR region, where the forest biome dominates, there is an increase of GPP (Figure 16.b.1) ranging from 0.1 to 5.0 μmolC m^{-2} s^{-1}, related to the aerosol effect, the lower values being associated with lower AOD values (Figure 8) and drier soil (Figure 5). In the remaining regions, the aerosol impact on GPP is still positive but much lower ($0.1 - 0.5$ μmolC m^{-2} s^{-1}). In all domains,

25 the majority of the aerosol impact is related to the increase in the diffuse fraction of solar radiation due to the presence of aerosols ($\%GPP_{diff} > 95\%$). As a general rule, our model results indicate that the increase of GPP leads to an increase ranging between 0.2 to 1.6 μmolC m^{-2} s^{-1} on plant respiration (R_P) for the forest and does not affect the other biomes significantly. On the other hand, soil respiration (R_H, line 3 of Figure 16) varies from 1 to 8 μmolC m^{-2} s^{-1}, with the higher values in the forest area with higher soil moisture (Figure 5). The aerosol impact on R_H is somewhat noisy, varying from -1

30 to +1 μmolC m^{-2} s^{-1} over the forest, negative otherwise (-0.1 μmolC m^{-2} s^{-1}). The noise of R_H is associated with the non-linear effects of aerosol on cloudiness (and thus temperature) and precipitation. The total impact of aerosol in NEE (line 4 of Figure 16) ranged from -0.1 to -5 μmolC m^{-2} s^{-1}, with the lower values found in the forest region with intense/persistent biomass burning, mainly related to the diffuse radiation effect, meaning that our modeling suggests that the aerosol biomass burning effect creates a CO_2 sink in *Amazônia*.

35

Total carbon fluxes in the *Amazônia*, weighted for the vegetation types: Figure 17 depicts the monthly mean diurnal cycle of the CO_2 fluxes in the LBAR for September 2010, again related to GPP, R_P, R_H, and NEE, averaged over the 4 types of vegetation present in each atmospheric model grid box. The presence of the biomass burning aerosol affects the CO_2 flux associated with GPP, and consequently Rp. Responding to the increasing diffuse radiation, both GPP and R_P rise, being the GPP enhancement about 4 times higher than the R_P. On contrast, RS has an opposite response as the presence of aerosol implies in a cooler soil (Figure 10) and, consequently, lower microbial activity. The net effect is a higher CO_2 daytime uptake, with a negligible night-time variation. Moreover, the biomass burning aerosol strongly impacts the NEE (Figure 17.b). Around noon, the NEE decreases from -7 to -10 $\mu molC\,m^{-2}\,s^{-1}$ in the presence of biomass burning, mainly due to the diffuse radiation effect. Nevertheless, it is interesting to note that the impact of the aerosol influence on the relative contribution of the diffuse to the total (diffuse + direct) on the NEE (Equation 4) has a different behavior depending on plant functional type, decaying exponentially as the AOD increases for all biomes, except for the C4 grass type. The contribution of the diffuse radiation effect to NEE ($\Delta NEE_{diff}/\Delta NEE_{tot}$) versus AOD, for each biome, is depicted in Figure 18 along with its fitting functions. Over forest, the percentage of the diffuse radiation effect on CO_2 uptake decreases exponentially ($[\Delta NEE_{diff}/\Delta NEE_{tot}]_{forest} \approx e^{-0.9AOD}, R^2 = 0.7$) from 100% to 50% with the increase of aerosol loading, reaching a balance of 50% - 50% between the diffuse and direct effect, for AOD above 0.5. For C3 grass and *cerrado*, as expected, the contribution of the diffuse radiation effects tends to zero with the increase of AOD ($[\Delta NEE_{diff}/\Delta NEE_{tot}]_{cerrado,C3} \approx 0.7e^{-4AOD}, R^2 = 0.7$). While for C4 grass type, the contribution of the diffuse radiation to NEE exponentially increases with AOD ($[\Delta NEE_{diff}/\Delta NEE_{tot}]_{C4} \approx e^{AOD}, R^2 = 0.9$), the C4 photosynthetic pathway does not rapidly saturate with the amount of light received. Considering the AOD underestimation of about 20% and the exponential behavior of the relative contribution of the diffuse fraction to NEE, it is reasonable to say that the contribution of the diffuse radiation effect on CO_2 uptake can reach 40% over the forest, and 10% over *cerrado* and C3 grass type, for high aerosol loads.

The model results for the CO_2 fluxes integrated for the month of September (2010), which is the peak of the burning season in the LBAR, are summarized in Table 4. Total modeled GPP in the LBAR is 1,113 Tg C, with the aerosol being responsible for an increase of 240 Tg C, with less than 1% due to the aerosol radiation direct effect. Plant respiration is affected by approximately 50 Tg C, related only to the increase in the diffuse fraction of radiation. The impact of the aerosol on the soil respiration is only 3% but in the opposite direction, i.e. a reduction. Integrating throughout the full month for September 2010, the NEE changed from +101 Tg C to -104 Tg C, when the aerosol effect is considered. The total aerosol effect on radiation was responsible for about 96% of the NEE change, while the temperature reduction due to the direct aerosol effect on radiation accounts for only 5%. That is, the aerosol effect, especially the change in the diffuse fraction of radiation, is strong enough to invert the signal of NEE, changing the ecosystem from being a source to a sink of CO_2. Table 3 shows that the NEE observed during the dry season at the Amazon forest and pasture biomes exhibit substantial site to site and interannual variability. Nevertheless, for each site, the 2010 model results are within the observed variability.

4   Conclusions and Final remarks

We conducted a modeling study during the peak of the burning season in *Amazônia* to assess the ability of a current state-of-the-art integrated in-line numerical atmospheric modeling system to simulate the CO_2 fluxes in *Amazônia*. A set of three different modeling experiments, first totally disregarding aerosol biomass burning effect, then considering only the direct aerosol effect, and, finally, also adding the aerosol effect on the diffuse fraction of radiation. The model results allowed us to assess and quantify the impacts of biomass burning aerosols on CO_2 fluxes in the Amazon Basin during the dry season. Moreover, the relative role of the main soil/vegetation and atmosphere interaction processes controlling the carbon cycle in *Amazônia* was weighed, and the aerosol effect on each of them was measured separately.

Consistent with previous studies (Freitas et al., 2005, 2009, and 2016; Longo et al., 2010, 2013; Rosário et al., 2013; Moreira et al., 2013), BRAMS performed well while modeling the meteorology and aerosol biomass burning emission, transport and removal processes in *Amazônia*, which has resulted in accurate simulation of the major features of AOD variability associated with the regional biomass burning plume over South America. The model results for surface temperature, rainfall and AOD were once again in agreement with observations for the 2010 dry season case study, representing the main characteristics of the spatial distribution and the diurnal cycle of temperature and precipitation. BRAMS was also evaluated on its performance to simulate CO and CO_2 mixing ratios using measurements acquired from air samples collected using light aircraft over the Amazon during 2010 and 2011 burning seasons. Typically, the model tends to slightly underestimate the CO mixing ratio, particularly in the lower levels, in regions affected by fresh biomass burning and haze biomass burning layers. Previous studies had already indicated an underestimation of the biomass burning emissions database used in this work (3BEM, Longo et al., 2010) of about 20% (Andreae et al., 2012), mainly related to fire omission and misrepresentation of the vegetation and carbon maps used (Pereira et al., 2016). For CO_2 mixing ratios, the comparison between model and observation is highly scattered, again especially in the lower levels, though in this case more likely related to convective activity pumping CO_2 to the upper layers of the atmosphere and inaccurate modeling of surface carbon net fluxes (NEE). In both cases, model inaccuracies are to be, at least partially, related to the lower model resolution (20 km), suggesting that further sensitivity studies on model resolution would be helpful. Nevertheless, although the 20-km model resolution was not capable of capturing CO_2 point measurements in *Amazônia*, the order of magnitude of the CO_2 mixing ratio has been in general well represented. Moreover, the diurnal cycle of CO_2 measured above the canopy of the *Tapajós* forest was represented in the model with differences of only about -0.9% and +1.4% between model results and observations during the time of minimum and maximum values, respectively.

Our modeling results indicate that during the dry season in *Amazônia*, regions with lower precipitation do not always have high values of NEE, because the lower soil respiration of a dryer soil can compensate for the deficit of water available for plants [e.g. Saleska, 2003]. Being an equatorial region, *Amazônia* receives abundant PAR. Therefore, areas with plenty of water availability in the soil have higher GPP compared to dry soil areas. However, after noon local time, when the radiation excess typically occurs, there is a drop in carbon assimilation for all biomes, except for the C4 grass type that has maximum assimilation coinciding with the peak of PAR.

The presence of an intense biomass burning aerosol layer during the dry season over *Amazônia* reduces the solar energy reaching the surface, consequently reducing near surface temperature. The model results show this cooling effect contributing to increasing the GPP in regions covered by forest, grass C3 and *cerrado*. However, in addition to reducing the surface energy, the aerosol layer also increases the diffuse fraction of radiation. This is the major effect that contributes to increasing GPP,

5 and, in this case, including the C4 grass type biome. These two effects altogether increase GPP of about 32%, 30%, 9% and 20% for forest, C3, and C4 type grasses, and *cerrado*, respectively.

In the LBAR, the GPP increased about 27%, reaching 1,113 TgC during September 2010, when the aerosol effects were included. Plant respiration also increased from 510 to 560 TgC, with the aerosol biomass burning effect as a response to the increase of GPP. The more CO_2 the plant assimilates to produce sugar, the more it needs to increase its respiration for

10 energy supply. On the other side, soil respiration dropped from 463 to 449 Tg C. Consequently, the NEE in the LBAR during September 2010 dropped from +101 to -104 TgC when the aerosol effects were considered, mainly due to the diffuse radiation effect. That is, the LBAR during the dry season, in the presence of high biomass burning aerosol loads, change from being a source to be a sink of CO_2 to the atmosphere. These results are also consistent with the observations of Yamasoe et al. (2006), who found no correlation between NEE and aerosol load for low AOD values (< 0.7); however, for AOD > 0.7 NEE values

15 became negative, and for AOD > 1.5-2 NEE started to increase again. Our model results also indicate that the impact of the aerosol on the NEE change is mainly related to the aerosol increasing the diffuse fraction of radiation. For AOD higher than 0.5, the forest reaches a balance of 50% – 50% between the diffuse and direct aerosol effects. For C3 grass type and *cerrado*, as expected, the contribution of the diffuse radiation effect is much lower than for the forest biome and tends to near zero with the increase of AOD. Direct measurements at the *Tapajós* site (Doughty et al., 2010) led to an estimation of the relative aerosol

20 contribution in CO_2 uptake, for high values of AOD, of 80% as a result of increased shaded light in the sub-canopy, related to the effect of aerosol increasing the diffuse fraction of radiation. While only 20% of the aerosol impact on CO_2 uptake was attributed to the decreased of canopy temperature. These same authors, however, do recognize that is "difficult to know whether this proportion is applicable to forest biomes worldwide or limited to tropical forest". So, based on our model results, we go even further and say that it is difficult to even to affirm that there is a unique rule applicable to the all Amazon forest due to its

25 high diversity of plant and soil charateristics, and microclimates.

Considering that the fire activity in *Amazônia* typically last for about 3 months, we can estimate as first approximation that the net impact of the biomass burning aerosols on the carbon cycle in *Amazônia* is about -615 TgC per year. However, we must say that the fire activity in 2010 was very intense (see Figure S.7 of the Supplementary document), and therefore, this estimation is not likely to be representative of an average year. According to Espírito-Santo et al. (2014), the impact of the natural disturbance

30 in the carbon cycle in *Amazônia* is generally around 1,300 TgC per year. Thus, the aerosol (negative) impact can be of a similar order of magnitude of the (positive) impact of the natural disturbances in the carbon cycle in *Amazônia*.

Our model results emphasize the importance of considering the effects of aerosol in numerical models of climate forecasting, especially when investigating the intensification of the greenhouse effect due to the atmospheric CO_2 concentration. In general, the numerical results obtained were in good agreement with observational data, including meteorological, aerosol and trace

35 gases variables, which gives us confidence in the estimation of the carbon fluxes. However, we do recognize that including the

effect of cloudiness on the diffuse fraction of radiation is an essential model capability that will allow us to explore the relative impact of the biomass burning aerosol and clouds, as well as the seasonality and the annual variability of the carbon cycle in Amazon. This is a work on development and we will soon report the inclusion of the cloud effect on the diffuse fraction of solar radiation in the model, which is certainly a major effect on the CO_2 budget in *Amazônia* during the wet season.

5　In addition, further model development based on current level of knowledge could still improve the representation of biomass burning aerosol effects in the carbon cycle. As such, model studies that include the reduction of photosynthesis due to the oxidation of plant leaves by high levels of ozone secondarily produced in biomass burning plumes, as well as the indirect aerosol effect on the CO_2 is a work in progress.

References

Akagi, S. K., Yokelson, R. J., Wiedinmyer, C., Alvarado, M. J., Reid, J. S., Karl, T., Crounse, J. D., and Wennberg, P. O.: Emission factors for open and domestic biomass burning for use in atmospheric models, Atmos. Chem. Phys., 11, 4039–4072, doi:10.5194/acp-11-4039-2011, 2011.

5 Andreae, M. O., Artaxo, P., Beck, V., Bela, M., Freitas, S., Gerbig, C., Longo, K., Munger, J. W., Wiedemann, K. T., and Wofsy, S. C.: Carbon monoxide and related trace gases and aerosols over the Amazon Basin during the wet and dry seasons, Atmos. Chem. Phys., 12, 6041–6065, doi:10.5194/acp-12-6041-2012, 2012.

Andreae, M. O., Rosenfeld, D., Artaxo, P., Costa, A. A., Frank, G. P., Longo, K. M., and Silva-Dias, M. A. F.: Smoking rain clouds over the Amazon, Science, 303, 1337–1342, doi:10.1126/science.1092779, 2004.

10 Andreae, M. O., Artaxo, P. , Brandão, C. , Carswell, F. E., Ciccioli, P. , da Costa, A. L., Culf, A. D., Esteves, J. L., Gash, J. H.C., Grace, J. , Kabat, P. , Lelieveld, J. , Malhi, Y. , Manzi, A. O., Meixner, F. X., Nobre, A. D., Nobre, C. , Ruivo, M. d.L.P., Silva-Dias, M. A., Stefani, P. , Valentini, R. , von Jouanne, J. and Waterloo, M. J.: Biogeochemical cycling of carbon, water, energy, trace gases, and aerosols in Amazonia: The LBA-EUSTACH experiments, Journal of Geophysical Research: Atmospheres, 107, LBA 33-1–LBA 33-25, ISSN: 2156-2202 DOI: 10.1029/2001JD000524, 2002.

15 Andreae, M. and Merlet, P.: Emission of trace gases and aerosols from biomass burning, Global Biogeochem. Cy., 15, 4, 955–966, 2001.

Araujo, A. C., Dolman, A. J., Waterloo, M. J., Gash, J. H. C., Kruijt, B., Zanchi, F. B., de Lange, J. M. E., Stoevelaar, R., Manzi, A. O., Nobre, A. D., Lootens, R. N., and Backer, J.: The spatial variability of CO_2 storage and the interpretation of eddy covariance fluxes in central Amazonia, Agr. Forest Meteorol., 150, 226–237, 2010.

Araujo, A. C., Nobre, A. D., Kruijt, B., Elbers, J. A., Dallarosa, R., Stefani, P., von Randow, C., Manzi, A. O., Culf, A. D., Gash, J. H.
20 C., Valentini, R., and Kabat, P.: Comparative measurements of carbon dioxide fluxes from two nearby towers in a central Amazonian rainforest: the Manaus LBA site, J. Geophys. Res. Atmos., 107, 8090, doi:10.1029/2001jd000676, 2002.

Baldocchi, D.: Measuring and modelling carbon dioxide and water vapour exchange over a temperate broad-leaved forest during the 1995 summer drought, Plant, Cell & Environment, 20, 1108-1122, ISSN: 1365-3040 DOI: 10.1046/j.1365-3040.1997.d01-147.x, 1997.

Batjes, N. H.: Documentation to ISRIC-WISE Global Data Set of Derived Soil Properties on a 1/2 Deg by 1/2 Deg Grid (Version 1.0),
25 Working Paper and Preprint 96/05, ISRIC, Wageningen, 1996.

Best, M. J., Pryor, M., Clark, D. B., Rooney, G. G., Essery, R .L. H., Ménard, C. B., Edwards, J. M., Hendry, M. A., Porson, A., Gedney, N., Mercado, L. M., Sitch, S., Blyth, E., Boucher, O., Cox, P. M., Grimmond, C. S. B., and Harding, R. J.: The Joint UK Land Environment Simulator (JULES), model description – Part 1: Energy and water fluxes, Geosci. Model Dev., 4, 677–699, doi:10.5194/gmd-4-677-2011, 2011.

30 Cirino, G. G., Souza, R. F., Adams, D. K., and Artaxo, P.: The effect of atmospheric aerosol particles and clouds on Net Ecosystem Exchange in Amazonia, Atmospheric Chemistry and Physics, 14, 6523-6543, 2014.

Clark, D. B., Mercado, L. M., Sitch, S., Jones, C. D., Gedney, N., Best, M. J., Pryor, M., Rooney, G. G., Essery, R. L. H., Blyth, E., Boucher, O., Harding, R. J., Huntingford, C., and Cox, P. M.: The Joint UK Land Environment Simulator (JULES), model description – Part 2: Carbon fluxes and vegetation dynamics, Geosci. Model Dev., 4, 701–722, doi:10.5194/gmd-4-701-2011, 2011.

35 Cochrane, M.A., Laurance, W.F.: Synergisms among fire, land use, and climate change in the Amazon, Ambio 37: 522-527, 2008.

Collatz, G. J., Ball, J. T., Grivet, C., and Berry, J. A.: Physiological and environmental regulation of stomatal conductance, photosynthesis and transpiration: a model that includes a laminar boundary layer, Agr. Forest Meteorol., 54, 107–136, doi:10.1016/0168-1923(91)90002-8, 1991.

Crassier, V., Suhre, K., Tulet, P., and Rosset, R.: Development of a reduced chemical scheme for use in mesoscale meteorological models, Atmos. Environ., 34, 2633–2644, 2000.

Dai, Y. J., Dickinson, R. E. & Wang, Y. P.: A two-big-leaf model for canopy temperature, photosynthesis, and stomatal conductance. J. Clim. 17, 2281–2299, 2004.

Doughty, C. E., Flanner, M. G. and Goulden, M. L.: Effect of smoke on subcanopy shaded light, canopy temperature, and carbon dioxide uptake in an Amazon rainforest, Global Biogeochemical Cycles, 24, ISSN: 1944-9224 DOI: 10.1029/2009GB003670, 2010.

Duncan, B. N. and Logan, J. A.: Model analysis of the factors regulating the trends and variability of carbon monoxide between 1988 and 1997, Atmos. Chem. Phys., 8, 7389–7403, doi:10.5194/acp-8-7389-2008, 2008.

Espírito-Santo, F. D. B., Gloor, M., Keller, M., Malhi, Y., Saatchi, S., Nelson, B., Oliveira Junior, R. C., Pereira, C., Lloyd, J., Frolking, S., Palace, M., Shimabukuro, Y. E., Duarte, V., Mendoza, A. M., López-González, G. L., Baker, T. R., Feldpausch, T.R., Brienen, R. J. W., Asner, G. P., Boyd, D. S., Phillips, O. L.: Size and frequency of natural forest disturbances and the Amazon forest carbon balance, Nat. Commun. 5:3434 doi: 10.1038/ncomms4434, 2014.

Feeley, K. J., Joseph Wright, S., Nur Supardi, M. N., Kassim, A. R. and Davies, S. J.: Decelerating growth in tropical forest trees, Ecology Letters, 10, 461-469, ISSN: 1461-0248 DOI: 10.1111/j.1461-0248.2007.01033.x, 2007.

Freitas, S. R., Longo, K. M., Silva Dias, M. A.F., Silva Dias, P. L., Chatfield, R., Prins, E., Artaxo, P., Grell, G. A. and Recuero, F. S.: Monitoring the transport of biomass burning emissions in South America, Environmental Fluid Mechanics, 5, 135-167, ISSN: 1567-7419 DOI: 10.1007/s10652-005-0243-7, 2005.

Freitas, S.R., Panetta, J., Longo, K.M., Rodrigues, L. F., Moreira, D. S., Rosário, N. E., Silva Dias, P. L., Silva Dias, M. A. F., Souza, E. P., Freitas, E. D., Longo, M., Frassoni, A., Fazenda, A. L., Santos e Silva, C. M., Pavani, C. A. B., Eiras, D., França, D. A., Massaru, D., Silva, F. B., Cavalcante, F., Pereira, G., Camponogara, G., Ferrada, G. A., Campos Velho, H. F., Menezes, I., Freire, J. L., Alonso, M. F., Gácita, M. S., Zarzur, M., Fonseca, R. M., Lima, R. S., Siqueira, R. A., Braz, R., Tomita, S., Oliveira, V., and Martins, L D.: The Brazilian developments on the Regional Atmospheric Modeling System (BRAMS 5.2): an integrated environmental model tuned for tropical areas, Geosci. Model Dev. Discuss., doi:10.5194/gmd-2016-130, 2016.

Freitas, S. R., Longo, K., Trentmann, J., Latham, D.: Technical Note: Sensitivity of 1D smoke plume rise models to the inclusion of environmental wind drag. Atmos. Chem. Phys., 10, 585, 2010.

Freitas, S. R., Longo, K. M., Silva Dias, M. A. F., Chatfield, R., Silva Dias, P., Artaxo, P., Andreae, M. O., Grell, G., Rodrigues, L. F., Fazenda, A., and Panetta, J.: The Coupled Aerosol and Tracer Transport model to the Brazilian developments on the Regional Atmospheric Modeling System (CATT-BRAMS) – Part 1: Model description and evaluation, Atmos. Chem. Phys., 9, 2843–2861, doi:10.5194/acp-9-2843-2009, 2009.

Freitas, S. R., K. M. Longo, R. Chatfield, et al.: Including the sub-grid scale plume rise of vegetation fires in low resolution atmospheric transport models. Atmos. Chem. Phys., 7, 3385 2007.

Gatti, L. V., Miller, J. B., D'Amelio, M. T. S., Martinewski, A., Basso, L. S., Gloor, M. E., Wofsy, S., and Tans, P.: Vertical profiles of CO_2 above eastern Amazonia suggest a net carbon flux to the atmosphere and balanced biosphere between 2000 and 2009, Tellus B, 62, 581–594, doi:10.1111/j.1600-0889.2010.00484.x, 2010.

Gevaerd, R. and Freitas, S. R.: Estimativa operacional da umidade do solo para inicializaçãao de modelos de previssão numérica da atmosfera. Parte I: Descrição da metodologia e validação, Revista Brasileira de Meteorologia, 21, 1–15, 2006 (in Portuguese).

Giglio, L., Descloitres, J., Justice, C. O., and Kaufman, Y. J.: An enhanced contextual fire detection algorithm for MODIS, Remote Sens. Environ., 87, 273–282, 2003.

5   Grace, J., Lloyd, J., Mcintyre, J., Miranda, A. C., Meir, P., Miranda, H. S., Nobre, C., Moncrieff, J., Massheder, J., Malhi, Y., Wright, I., Gash, J.: Carbon dioxide uptake by an undisturbed tropical rain forest in southwest Amazonia, 1992 to 1993. Science, vol 270, 1995.

Grell, G. A., and Freitas, S.R.: A scale and aerosol aware stochastic convective parameterization for weather and air quality modeling. Atmos. Chem. Phys., 14, 5233, 2014.

Harrison, L., and Michalsky, J.: Objective algorithms for the retrieval of optical depths from ground-based measurements. Applied Optics, 10   33(22), 5126–5132, 1994.

Harrison, L., Michalsky, J., and Berndt, J.: Automated multifilter rotating shadow-band radiometer: an instrument for optical depth and radiation measurements. Applied Optics, 33(22), 5118–5125, 1994.

Hoelzemann, J. J., Longo, K. M., Fonseca, R. M., do Rosário, N. M., E., Elbern, H., Freitas, S. R., and Pires, C.: Regional representativity of AERONET observation sites during the biomass burning season in South America determined by correlation studies with MODIS Aerosol 15   Optical Depth, J. Geophys. Res., 114, D13301, doi:10.1029/2008jd010369, 2009.

Holben, B. N., Eck, T. F., Slutsker, I., Tanré, D., Buis, J. P., Setzer, A., Vermote, E., Reagan, J. A., Kaufman, Y. J., Nakajima, T., Lavenu, F., Jankowiak, I., and Smirnov, A.: AERONET – A Federated Instrument Network and Data Archive for Aerosol Characterization, Remote Sens. Environ., 66, 1–16, doi: 10.1016/s0034-4257(98)00031-5, 1998.

Holloway, T., Levy, H., and Kasibhatla, P.: Global distribution of carbon monoxide, J. Geophys. Res., 105, 12123–12147, 2000. Houghton, 20   R. A., Lawrence, K. T., Hackler, J. L., and Brown, S.: The spatial distribution of forest biomass in the Brazilian Amazon: a comparison of estimates, Glob. Change Biol., 7(7), 731–746, 2001.

Houghton, R. A., Lawrence, K. T., Hackler, J. L., and Brown, S.: The spatial distribution of forest biomass in the Brazilian Amazon: a comparison of estimates, Glob. Change Biol., 7(7), 731–746, 2001.

Hutyra, L. R., Munger, J. W., Saleska, S. R., Gottlieb, E., Daube, B. C., Dunn, A. L., Amaral, D. F., de Camargo, P. B. and Wofsy, S. C.: 25   Seasonal controls on the exchange of carbon and water in an Amazonian rain forest, 2007.

James, S. E., Poertel, M., Wilson, S. D. et al.: Temporal heterogeneity of soil moisture in grassland and forest. J. Ecol. 91: 234/239, 2003.

Kanniah, K. D., Beringer, J., North, P., Hutley, L.: Control of atmospheric particles on diffuse radiation and terrestrial plant productivity: A review. Progress in Physical Geography, 36(2), 209-237, 2012.

Kaufman, Y. J.: Remote sensing of direct and indirect aerosol forcing, in: Aerosol Forcing of Climate, edited by: Charlson, R. J. and 30   Heintzenberg, J., John Wiley & Sons, New York, 297–332, 1995.

Knohl, A. and Baldocchi, D. D.: Effects of diffuse radiation on canopy gas exchange processes in a forest ecosystem, Journal of Geophysical Research: Biogeosciences, 113, ISSN: 2156-2202 DOI: 10.1029/2007JG000663, 2008.

Kawanishi, T., Kuroiwa, H., Kojima, M., Oikawa, K., Kozu, T., Kumagai, H., Okamoto, K., Okumura, M., Nakatsuka, H., and Nishikawa, K.: TRMM precipitation radar, Adv. Space Res., 25, 969–972, doi:10.1016/S0273-1177(99)00932-1, 2000.

35   Krol, M. C., Hooghiemstra, P. B., van Leeuwen, T. T., van der Werf, G. R., Novelli, P. C., Deeter, M. N., Aben, I., and Röckmann, T.: Correction to "Interannual variability of carbon monoxide emission estimates over South America from 2006 to 2010": CORRECTIONS, J. Geophys. Res. Atmospheres, 118(10), 5061–5064, doi:10.1002/jgrd.50389, 2013.

Krol, M., Houweling, S., Bregman, B., van den Broek, M., Segers, A., van Velthoven, P., Peters, W., Dentener, F., and Bergamaschi, P.: The two-way nested global chemistry-transport zoom model TM5: algorithm and applications, Atmos. Chem. Phys., 5, 417–432, doi:10.5194/acp-5-417-2005, 2005.

Koren, I., Kaufman, Y. J., Remer, L. A., and Martins, J. V.: Measurement of the effect of Amazon smoke on inhibition of cloud formation, Science, 303, 1342–1345, doi:10.1126/science.1089424, 2004.

Kummerow, C., Olson, W. S., and Giglio, L.: A simplified scheme for obtaining precipitation and vertical hydrometer profiles from passive microwave sensors. IEEE Trans. Geosci. Remote Sens., 34, 1213–1232, 1996.

Longo, K. M., Freitas, S. R., Pirre, M., Marecal, V., Rodrigues, L. F., Panetta, J. , Alonso, M. F., Rosario, N. E., Moreira, D. S., Gácita, M. S., Arteta, J. , Fonseca, R. , Stockler, R. , Katsurayama, D. M., Fazenda, A. and Bela, M. : The Chemistry CATT-BRAMS model (CCATT-BRAMS 4.5): a regional atmospheric model system for integrated air quality and weather forecasting and research, Geoscientific Model Development, 6, 1389-1405, DOI: 10.5194/gmd-6-1389-2013, 2013.

Longo, K. M., Freitas, S. R., Andreae, M. O., Setzer, A., Prins, E., and Artaxo, P.: The Coupled Aerosol and Tracer Transport model to the Brazilian developments on the Regional Atmospheric Modeling System (CATT-BRAMS) – Part 2: Model sensitivity to the biomass burning inventories, Atmos. Chem. Phys., 10, 5785–5795, doi:10.5194/acp-10-5785-2010, 2010.

Longo, K., Freitas, S. R., Andreae, M.O., Yokelson, R., Artaxo, P.: Biomass burning in Amazonia: emissions, long range transport of smoke and Its regional and remote Impacts. In Amazonia and Global Change, by the American Geophysical Union Press. Eds. John Gash, Michael Keller, Mercedes Bustamante, Pedro Silva Dias, 2009.

Mellor, G. L. and Yamada, T.: Development of a turbulence closure model for geophysical fluid problems, Rev. Geophys., 20, 851–875, doi:10.1029/RG020i004p00851, 1982.

Mercado, L. M., Bellouin, N., Sitch, S., Boucher, O., Huntingford, C., Wild, M., and Cox, P. M.: Impact of changes in diffuse radiation on the global land carbon sink, Nature, 458, 1014–1017, doi:10.1038/nature07949, 2009.

Min, Q.: Impacts of aerosols and clouds on forest-atmosphere carbon exchange, Journal of Geophysical Research: Atmospheres, 110, ISSN: 2156-2202 DOI: 10.1029/2004JD004858, 2005.

Misson, L., Lunden, M., McKay, M. and Goldstein, A. H.: Atmospheric aerosol light scattering and surface wetness influence the diurnal pattern of net ecosystem exchange in a semi-arid ponderosa pine plantation, Agricultural and Forest Meteorology , 129, 69-83, ISSN: 0168-1923 DOI: http://dx.doi.org/10.1016/j.agrformet.2004.11.008, 2005.

Moreira, D. S., Freitas, S. R., Bonatti, J. P., Mercado, L. M., Rosário, N. M. É., Longo, K. M., Miller, J. B., Gloor, M. and Gatti, L. V.: Coupling between the JULES land-surface scheme and the CCATT-BRAMS atmospheric chemistry model (JULES-CCATT-BRAMS1.0): applications to numerical weather forecasting and the CO_2 budget in South America, Geoscientific Model Development Discussions, 6, 453-494, DOI: 10.5194/gmdd-6-453-2013, 2013.

Nepstad, D.C., Veríssimo, A., Alencar, A., Nobre, C., Lima, E., Lefebvre, P., Schlesinger, P., Potter, C., Moutinho, P., Mendoza, E.,, Cochrane, M., Brooks, V.: Large-scale impoverishment of Amazonian forests by logging and fire, Nature, 398, 505-508, 1999.

Oliveira, P. H. F., Artaxo, P., Pires, C., De Lucca, S., Procópio, A., Holben, B., Schafer, J., Cardoso, L. F., Wofsy, S. C., and Rocha, H. R.: The effects of biomass burning aerosols and clouds on the CO_2 flux in Amazonia. Tellus B 59, no. 3, 2007.

Olson, J. S.: Global Ecosystem Framework-Definitions, USGS EROS Data Center Internal Report, Sioux Falls, 37 pp., 1994.

Pereira, G., Siqueira, R., Rosário, N. E., Longo, K. M., Freitas, S. R., Cardozo, F. S., Kaiser, J. W., and Wooster, M. J.: Assessment of fire emission inventories during the South American Biomass Burning Analysis (SAMBBA) experiment. Atmos. Chem. Phys., 16, 6961–6975, doi:10.5194/acp-16-6961-2016, 2016.

Peters, W., Jacobson, A. R., Sweeney, C., Andrews, A. E., Conway, T. J., Masarie, K., Miller, J. B., Bruhwiler, L. M. P., Pétron, G., Hirsch, A. I., Worthy, D. E. J., van der Werf, G. R., Randerson, J. T., Wennberg, P. O., Krol, M. C., and Tans, P. P.: An atmospheric perspective on North American carbon dioxide exchange: CarbonTracker, P. Natl. Acad. Sci. USA, 104, 18925–18930, doi:10.1073/pnas.0708986104, 2007.

5 Prins, E. M., Feltz, J. M., Menzel, W. P., and Ward, D. E.: An overview of GOES-8 diurnal fire and smoke results for SCAR-B and 1995 fire season in South America, J. Geophys. Res., 103, 31821–31835, doi:10.1029/98JD01720, 1998.

Procópio, A. S., Remer, L. A., Artaxo, P., Kaufman, Y. J., and Holben, B. N.: Modeled spectral optical properties for smoke aerosols in Amazonia, Geophys. Res. Lett., 30, 2265, doi:10.1029/2003GL018063, 2003.

Procópio, A. S., Artaxo, P., Kaufman, Y. J., Remer, L. A., Schafer, J. S. and Holben, B. N.: Multiyear analysis of Amazonian biomass burning

10 smoke radiative forcing of climate, Geophysical Research Letters, 31, ISSN: 1944-8007 DOI: 10.1029/2003GL018646, 2004.

Rap, A., Spracklen, D. V., Mercado, L., Reddington, C. L., Haywood, J. M., Ellis, R. J., and Butt, N.: Fires increase Amazon forest productivity through increases in diffuse radiation. Geophysical Research Letters, 42(11), 4654-4662, 2015.

Reid, J.S., Koppmann, R., Eck, T.F., Eleuterio, D.P.: A review of biomass burning emissions part II: intensive physical properties of biomass burning particles. Atmos. Chem. Phys 5 (3), 799–825, 2005.

15 Reynolds, R. W., Rayner, N. A., Smith, T. M., Stokes, D. C., and Wang, W.: An improved in situ and satellite SST analysis for climate, J. Climate, 15, 1609–1625, doi:10.1175/1520-0442(2002)0152.0.CO;2, 2002.

Rosário, N., Yamasoe, M. A., Sayão, A. and Siqueira, R.: Multifilter rotating shadowband radiometer calibration for spectral aerosol optical depth retrievals over *São Paulo* City, Brazil. Applied Optics 47(9), 1171-1176, 2008.

Rosário, N. E., Longo, K. M., Freitas, S. R., Yamasoe, M. A., and Fonseca, R. M.: Modeling the South American regional smoke plume:

20 aerosol optical depth variability and surface shortwave flux perturbation, Atmos. Chem. Phys., 13, 2923–2938, doi:10.5194/acp-13-2923-2013, 2013.

Rosário, N. M. E.: Variability of aerosol optical properties over South America and the impacts of direct radiative effect of aerosols from biomass burning, Ph.D. thesis, Institute of Astronomy, Geophysics and Atmospheric Sciences, University of *São Paulo*, *São Paulo*, 2011 (in Portuguese).

25 Rosenfeld, D.: TRMM observed first direct evidence of smoke from forest fires inhibiting rainfall, Geophys. Res. Lett., 26, 3105–3108, 1999.

Rossato, L., Alvalá, R. C. S., and Tomasella, J.: Distribuição geográfica da capacidade de armazenamento de água e das propriedades físicas do solo no Brasil, in: X Congresso Brasileiro de Meteorologia/VIII Congresso da FLISMET, Brasília, DF, Brazil, 1998 (in Portuguese).

Saleska, S. R., Miller, S. D., Matross, D. M., Goulden, M. L., Wofsy, S. C., da Rocha, H. R., de Camargo, P. B., Crill, P., Daube, B. C., de Freitas, H. C., Hutyra, L., Keller, M., Kirchhoff, V., Menton, M., Munger, J. W., Pyle, E. H., Rice, A. H., and Silva, H.: Carbon in Amazon

30 forests: unexpected seasonal fluxes and disturbance-induced losses, Science, 302, 1554–1557, 2003.

Schafer, J. S., T. F. Eck, B. N. Holben, P. Artaxo, and A. F. Duarte (2008), Characterization of the optical properties of atmospheric aerosols in Amazônia from long-term AERONET monitoring (1993–1995 and 1999–2006), J. Geophys. Res., 113, D04204, doi:10.1029/2007JD009319.

Stockwell, W. R., Kirchner, F., and Kuhn, M.: A new mechanism for regional chemistry modeling, J. Geophys. Res., 102, 25847– 25879,

35 1997.

Sestini, M. F., Reimer, E. S., Valeriano, D. M., Alvalá, R. C.S., Mello, E. M.K., Chan, C. S. and Nobre, C. A.: Mapa de cobertura da terra da Amazônia legal para uso em modelos meteorológicos, In: Anais do Simpósio Brasileiro de Sensoriamento Remoto, 11. (SBSR), Belo Horizonte, 2901-2906, 2003.

Setzer, A. and Pereira, M.: Amazonia biomass burnings in 1987 and an estimate of their tropospheric emissions, Ambio, 20, 19–22, 1991.

Sitch, S., Cox, P. M., Collins, W. J., and Huntingford, C.: Indirect radiative forcing of climate change through ozone effects on the land-carbon sink, Nature, 448, 791–794, doi:10.1038/nature06059, 2007.

Steiner, A. and Chameides, W.: Aerosol-induced thermal effects increase modelled terrestrial photosynthesis and transpiration, Tellus B, 57, ISSN: 1600-0889, 2011.

Tans, P. P., Bakwin, P. S. and Guenther, D. W.: A feasible global carbon cycle observing system: a plan to decipher today's carbon cycle based on observations. Glob. Chang. Biol. 2, 309–318, 1996.

Toon, O. B., Turco, R. P., Westphal, D., Malone, R. and Liu, M.: A Multidimensional Model for Aerosols: Description of Computational Analogs, J. Atmos. Sci., 45, 2123-2144, ISSN: 0022-4928 DOI: 10.1175/1520-0469(1988)0452.0.CO;2, 1988.

Toon, O. B., McKay, C. P., Ackerman, T. P., and Santhanam, K.: Rapid calculation of radiative heating rates and photodissociation rates in inhomogeneous multiple scattering atmospheres, J. Geophys. Res., 94, 16287–16301, doi:10.1029/JD094iD13p16287, 1989.

von Randow, C., Manzi, A. O., Kruijt, B., de Oliveira, P. J., Zanchi, F. B., Silva, R. L., Hodnett, M. G., Gash, J. H. C., Elbers, J. A., Waterloo, M. J., Cardoso, F. L., and Kabat, P.: Comparative measurements and seasonal variations in energy and carbon exchange over forest and pasture in South West Amazonia, Theor. Appl. Climatol., 78, doi:10.1007/s00704-004-0041-z, 2004.

Vourlitis, G. L., de Almeida Lobo, F., Zeilhofer, P., and de Souza Nogueira, J.: Temporal patterns of net CO_2 exchange for a tropical semideciduous forest of the southern Amazon Basin, J. Geophys. Res., 116, G03029, doi:10.1029/2010JG001524, 2011.

Walko, R. L., Cotton, W. R., Meyers, M. P., and Harrington, J. Y.: New RAMS cloud microphysics parameterization. Part I: the single-moment scheme, Atmos. Res., 38, 29–62, doi: 10.1016/0169-8095(94)00087-T, 1995.

Yamasoe, M. A., von Randow, C., Manzi, A. O., Schafer, J. S., Eck, T. F., and Holben, B. N.: Effect of smoke and clouds on the transmissivity of photosynthetically active radiation inside the canopy, Atmos. Chem. Phys., 6, 1645–1656, doi:10.5194/acp-6-1645-2006, 2006.

Yarwood, G., Rao, S., Yocke, M., and Whitten, G. Z.: Updates to the Carbon Bond chemical mechanism: CB05, Final Report to the US EPA, RT-0400675, Novato, CA, available at: http://www.camx.com/files/cb05_final_report_120805.aspx, last access: 19 July 2016, 2005.

Yu, H., Lui, S. C. and Dickinson, R. E.: Radiative effects of aerosols on the evolution of the atmospheric boundary layer, J. Geophys. Res., 107(D12), doi:10.1029/2001JD000754, 2002.

Zobler, L.: Global Soil Types, 1-Degree Grid (Zobler), data set, available at: http://www.daac.ornl.gov from Oak Ridge National Laboratory Distributed Active Archive Center, Oak Ridge, Tennessee, USA, doi:10.3334/ORNLDAAC/418, 1999.

Table 1. Parameters for a third-degree polynomial fit to the diffuse fraction of broadband solar irradiance reaching the surface as function of AOD at 670 nm for distinct air mass intervals.

Optical air mass	a	b	c	d	R^2
m ≤ 1.10	0.0115	-0.1115	0.4693	0.1258	0.994
1.10 < m ≤ 1.25	0.0129	-0.1235	0.4997	0.1304	0.994
1.25 < m ≤ 1.40	0.0075	-0.1087	0.5035	0.1477	0.989
1.40 < m ≤ 1.70	0.0052	-0.1031	0.5077	0.1795	0.990
1.70 < m ≤ 2.00	0.0144	-0.1634	0.6207	0.1696	0.991
2.00 < m ≤ 2.80	0.0166	-0.2237	0.7458	0.1851	0.981
m > 2.80	0.0736	-0.4631	1.0152	0.2005	0.985

Table 2. Monthly mean values of net GPP, ΔGPP_{tot} and ΔGPP_{dir} in the LBAR during September 2010 for the three simulations and different biomes.

2*Biome	$GPP_{DIR+DIF}$	ΔGPP_{tot}		ΔGPP_{dir}	
	$[\text{TgCmonth}^{-1}]$	$[\text{TgCmonth}^{-1}]$	$[\%]$	$[\text{TgCmonth}^{-1}]$	$[\%]$
Forest	1,206	293	32	8	1
C3G	850	195	30	24	3
C4G	2,431	200	9	-69	-3
Cerrado	359	59	20	12	3

Table 3. NEE measurements during the dry season in several locations in the Amazon region, Brazil. The mean values and standard deviation of NEE from the modeling results from DIR+DIF experiment (September 2010) are also presented in the last column.

Loca	Biome type	Data collection period	NEE from flux measurements			NEE from the model (Sept 2010)		
			Daily total $molCm^{-2}day^{-1}$	Nighttime $\mu molCm^{-2}s^{-1}$	Daytime peak $\mu molCm^{-2}s^{-1}$	Daily total $molCm^{-2}day^{-1}$	Nighttime $\mu molCm^{-2}s^{-1}$	Daytime peak $\mu molCm^{-2}s^{-1}$
Jaru[a]	3*Forest	Sept 1992	-0.090	-	-	3*-0.065 ±0.002	3*+5.2 ±0.8	3*-11.9 ±2.4
Jaru[b1]		dry season 1999-2002	-0.069	+7.1	-17.5			
FNS[b2]	Pasture	Dry season 1999-2002	-0.12	+3.0	-13.2	-0.14* ±0.1	+3.3 ±0.8	-13.1 ±5.4
4*_Tapajós_	4*Forest	Sept 2002	+0.017	-	-	4*-0.032 ±0.039	4*+5.6 ±0.9	4*-11.9 ±0.6
		Sept 2003	+ 0.026	-	-			
		Sept 2004	-0.017	-	-			
		Sept 2005	-0.069	-	-			
5*Sinop[d]	5*Forest	Dry season 2005–2006	+0.008 ±0.029	+5.2 ±0.4	-	5*-0.23 ±0.006	5*+3.0 ±0.3	5*-14.4 ±1.0
		Dry season 2006–2007	-0.013 ±0.024	+5.5 ±0.4	-			
		Dry season 2007–2008	-0.041 ±0.022	+5.6 ±0.3	-			
Cuieiras[e]	Forest	Dry season 1999-2009	-	~+4.0	-20.0	+0.037 ±0.015	+6.8 ±1.0	-11.7 ±1.4

[a] Jaru reserve (10°05'S, 61°57'W), Grace et al., 1995.

[b1] Jaru reserve (10°05'S, 61°57'W), Von Randow et al., 2004.

[b2] Fazenda Nossa Senhora (10°45'44"S,62°21'27"W), Von Randow et al., 2004.

[c] _Tapajós_ National Forest (2°51'S,54°58'W), Hutyra et al., 2007.

[d] 50 km NE of Sinop-MT (11°25'S, 55°20'W), Vourlitis et al., 2011.

[e] Cuieiras Biological Reserve (2°36'33" S, 60°12'33" W), Cirino et al., 2015.

* The pasture site was identified as C4 grass type.

Table 4. Total CO_2 assimilation ratio for the DIR+DIF simulation, $\Delta Flux_{tot}$ and $\Delta Flux_{dir}$ in the LBAR during September 2010 for the different atmosphere-biosphere exchange processes.

2*Process	CO_2 $Flux$	$\Delta Flux_{tot}$		$\Delta Flux_{dir}$	
	[TgCmonth^{-1}]	[TgCmonth^{-1}]	[%]	[TgCmonth^{-1}]	[%]
GPP	1,113	240	27	1	0
R_p	560	50	10	0	0
R_H	449	-14	-3	-7	-2
NEE	-104	-205	-203	-8	8
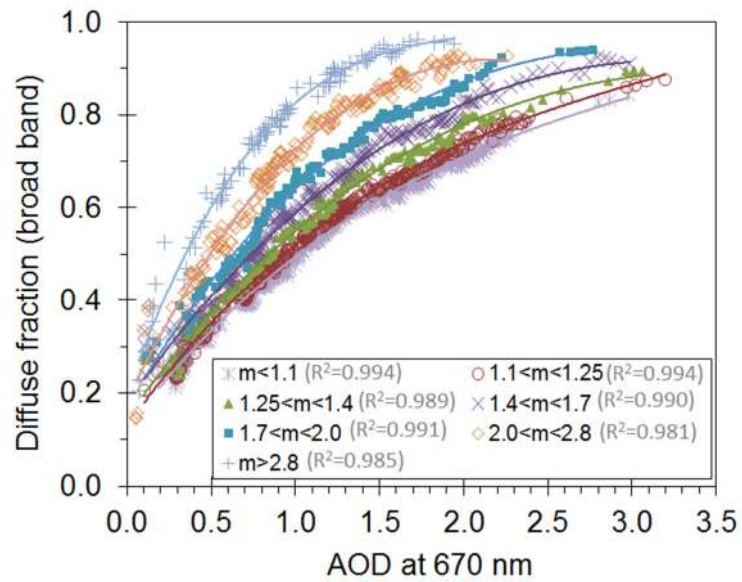
Figure 1. Fraction of diffuse broadband solar irradiance reaching the surface as function of AOD at 670 nm and optical air mass intervals (m).
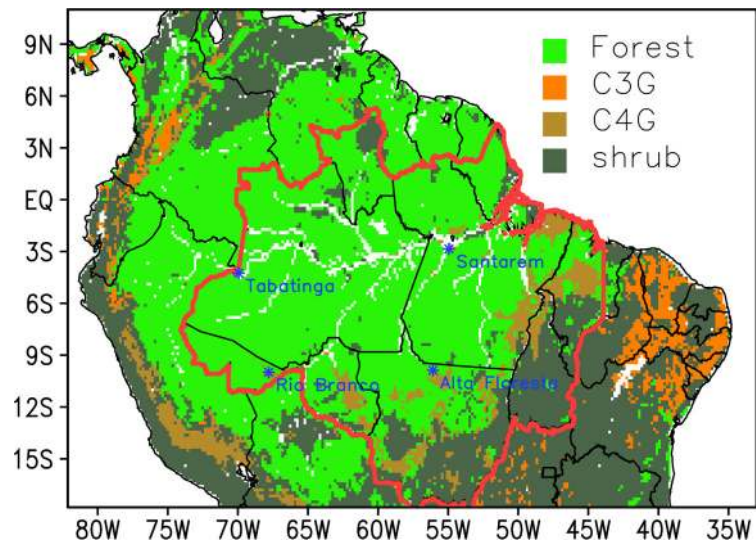
Figure 2. Model domain with the map of land cover used in BRAMS, the color scale depicting the dominant biomes. The red contour line on the map delimits the LBAR and the locations of CO_2 and CO airborne measurements: *Santarém*, PA (2.85° S, 54.95° W); *Rio Branco*, AC (9.99° S, 67.80° W); *Alta Floresta*, MT (9.87° S, 56.09° W); and *Tabatinga*, AM (4.25° S, 69.94° W).
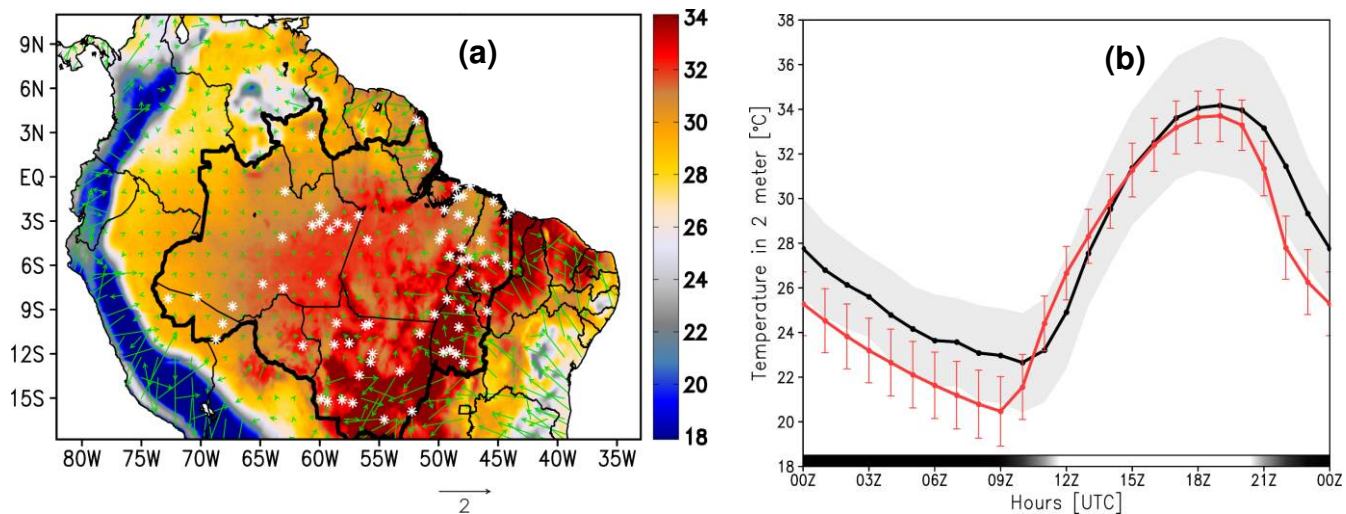
Figure 3. (a) Spatial distribution of mean 2-meter temperature and 10-meter wind field from the model during September 2010 at 1600 UTC. The LBAR and the locations of 72 near-surface measurement ground stations, used to evaluate the model 2-meter temperature, are depicted in the map with white asterisks. (b) Mean diurnal cycle of 2-meter temperature (°C) observed in the 72 near-surface ground stations (black line) and from the model grid-point nearest the respective station (red line). The standard deviation (shaded gray) and the mean observed temperature values were calculated using measurements at the 72 observational stations. While the model standard deviation (red bars) and mean temperature were calculated using the model temperatures at the gridboxes corresponding to the locations of the 72 stations.
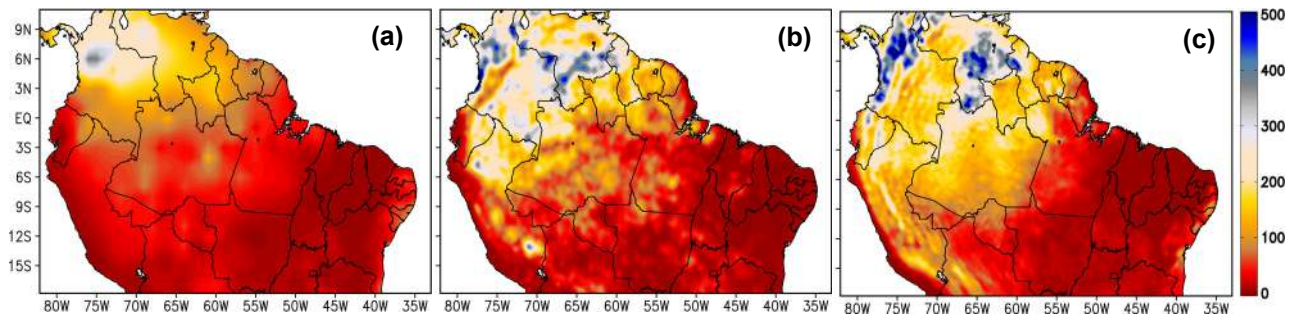
Figure 4. Accumulated precipitation (mm) during September 2010 from the (a) ground stations observation network interpolated for the model grid point, (b) TRMM rainfall product, and (c) model results.
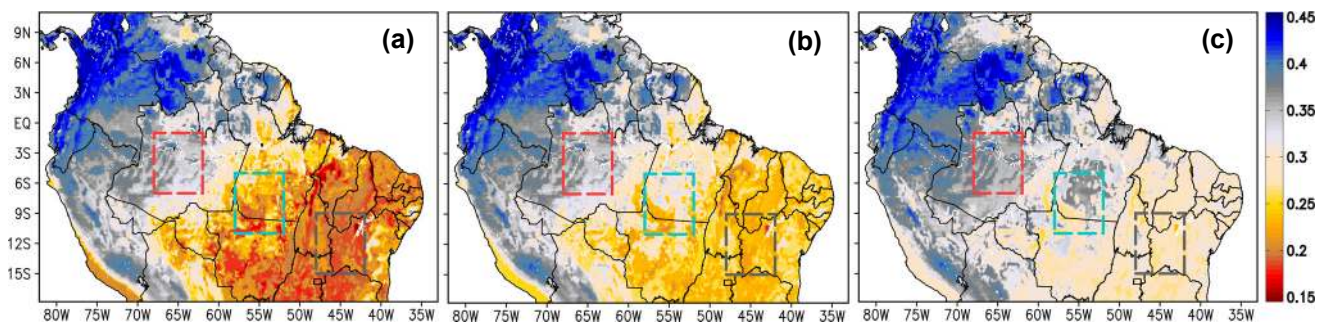
Figure 5. Monthly mean soil moisture ($m^3 m^{-3}$) during September 2010 at three soil levels: (a) 0.35 m, (b) 1.00 m, and (c) 4.25 m. The rectangles depict areas with predominance of forest and moist soil (red), forest and dry soil (blue), and *cerrado* with dry soil (gray).
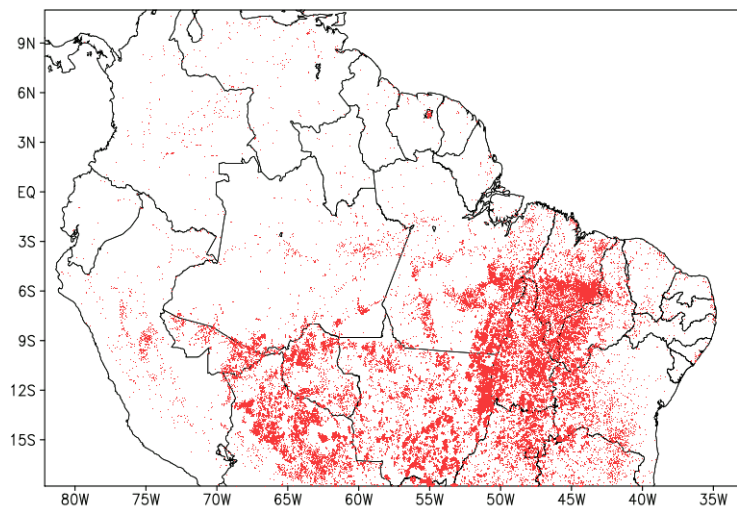
Figure 6. Burning points observed by the AVHRR sensor during September 2010. (Source: www.cptec.inpe.br/queimadas).
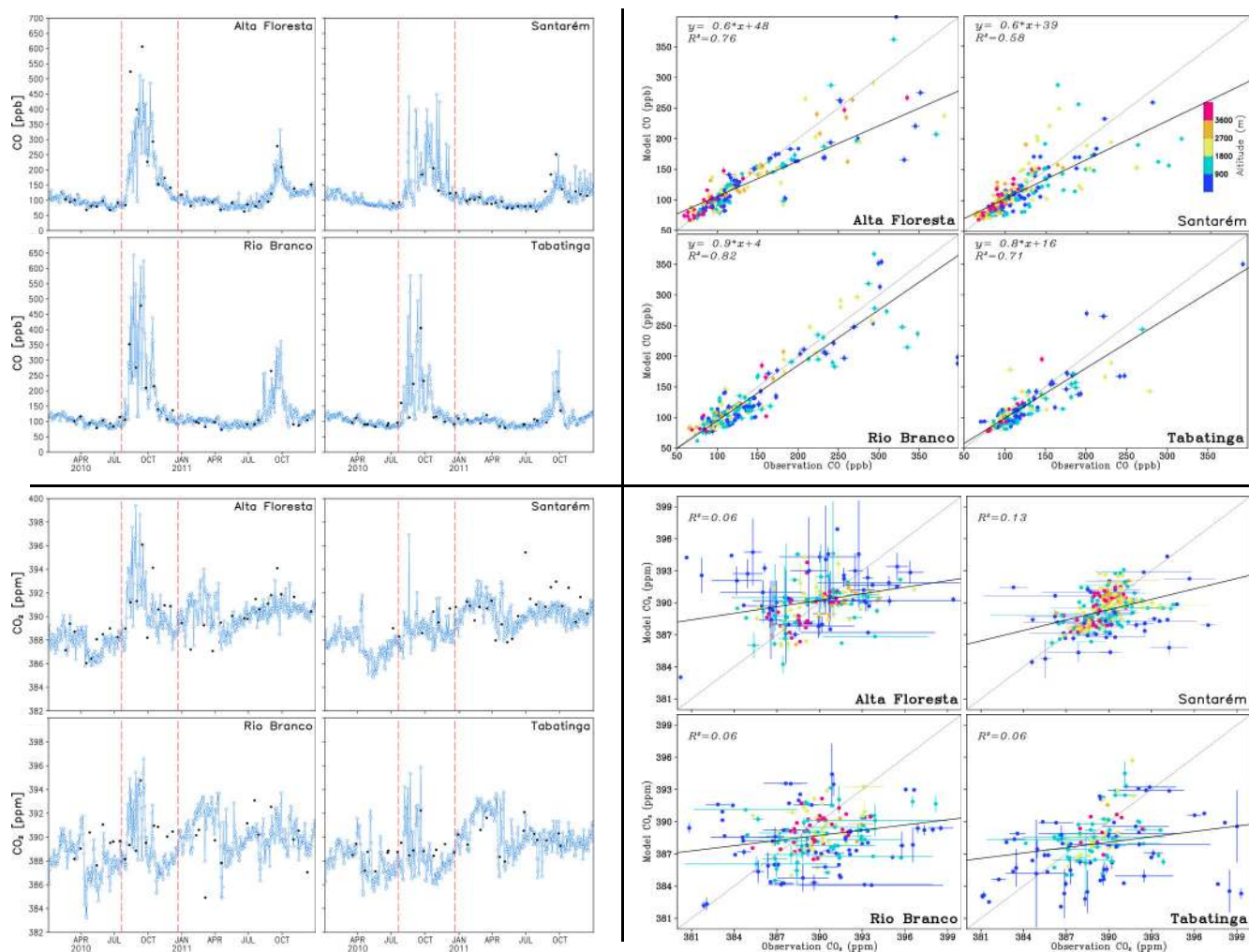
Figure 7. Time series (on the left) and scatter plots (on the right) of CO (ppbv) (on the top) and CO_2 (ppbv) (on the bottom) airborne measured (black dots) and simulated (DIR+DIF experiment, blue dots and line) at *Alta Floresta*, *Santarém*, *Rio Branco*, and *Tabatinga* (indicated on each plot), at about 2 km above the ground level from April 2010 to October 2011. On the time series, the red dashed lines on the time series indicate the fire season of 2010. On the scatter plots, the colors scale depicts the vertical layers: < 900 m (purple), 900-1800 m (blue), 1800-2700 (green), 2700-3600 (orange), and > 3600 m (pink), and the error bars refer to the standard deviation of the mean values. The locations of the measurement sites are indicated in Figure 2.
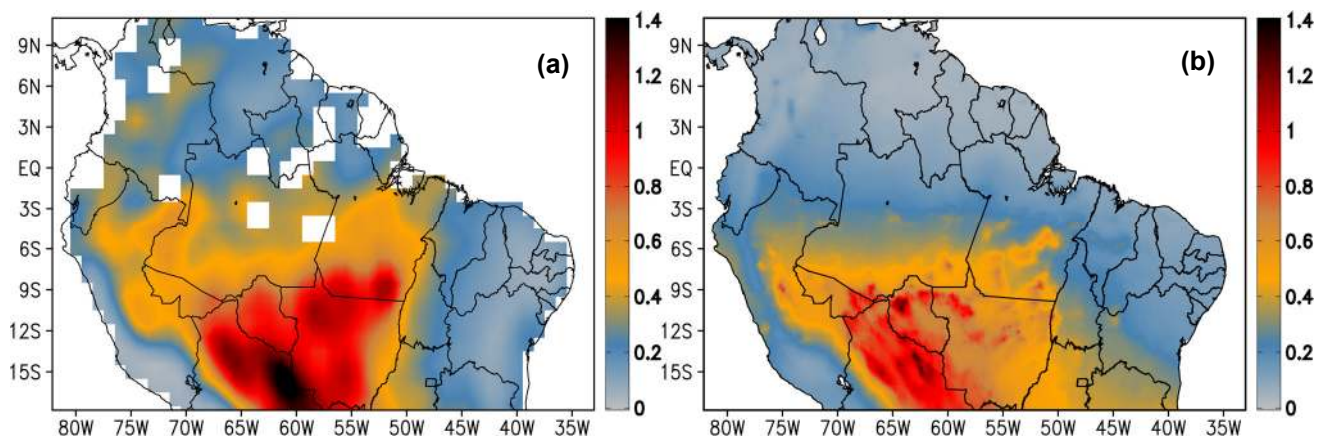
Figure 8. Monthly mean AOD at 550 nm wavelength for September 2010 from (a) MODIS Aqua retrieval, and (b) from the model as simulated on the DIR+DIF experiment.
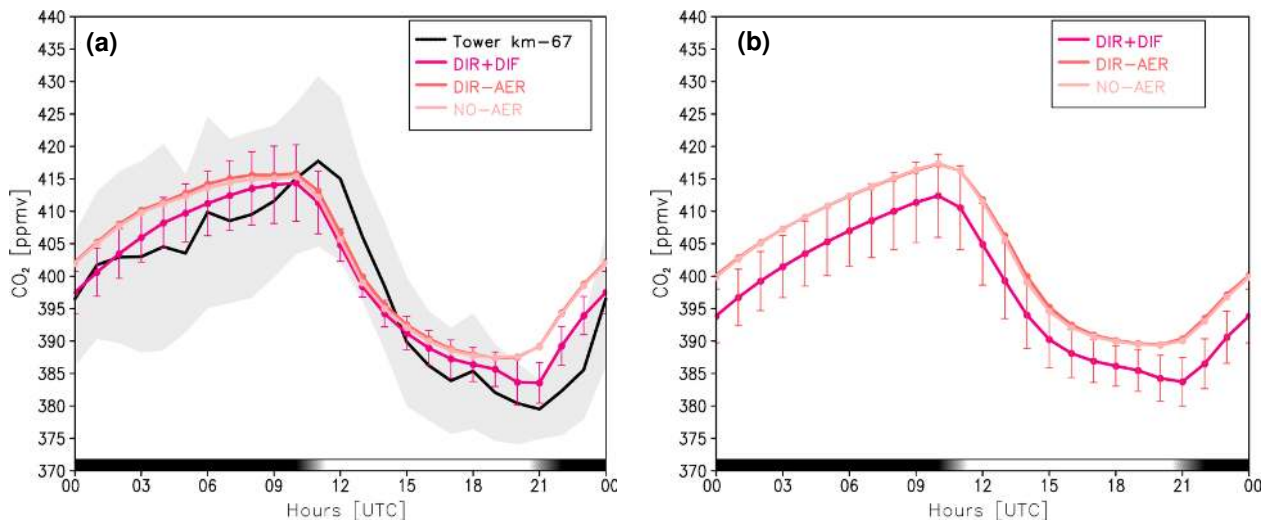
Figure 9. (a) Mean diurnal cycle of CO_2 (ppmv) mixing ratio (black line) during September 2010 in *Tapajós* forest tower at 39.6 meter (2.85° S, 55.04° W, slightly southward *Santarém*, location indicated in Figure 2). The gray shaded area indicates the standard deviation of mean values observed. (b) Mean diurnal cycle of CO_2 (ppmv) mixing ratio from the model during the same period in the LBAR (red line in Figure 2). In both plots, model results are at the 39.3 meters' model level for the three simulations NO-AER (light pink), DIR-AER (pink), and DIR+DIF (red). The red error bars on the model curves refer to the standard deviation of the mean model values.

41
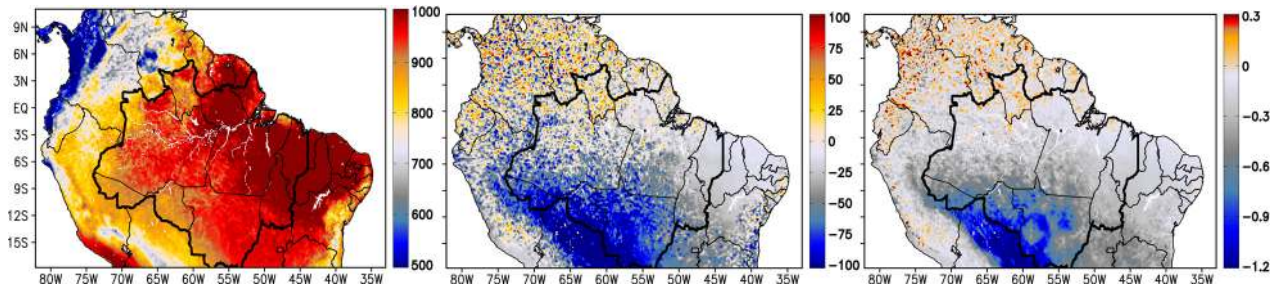
Figure 10. (a) Mean downwelling shortwave irradiance at the surface (Wm^{-2}) at 1600 UTC (which is around midday in most of Amazonia) for September 2010 from DIR+DIF experiment; (b) the difference in the mean downwelling shortwave irradiance at the surface (Wm^{-2}) during the same time period as simulated at DIR+DIF and NO-AER; and (c) the difference in the 2-meter temperature ($^{\circ}$C) during the same time period as simulated at DIR+DIF and NO-AER. The darker black contour line on the maps delimits the LBAR.
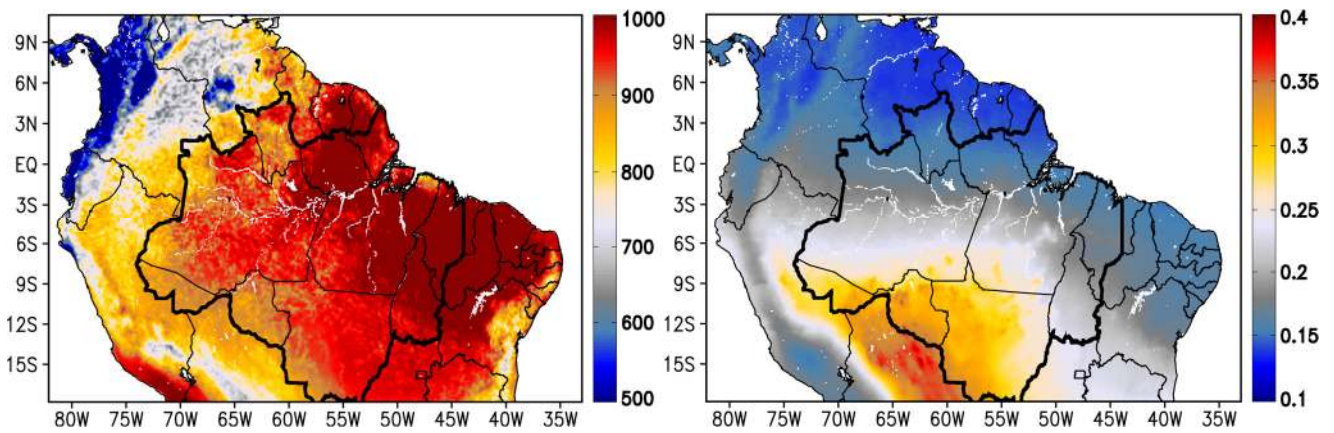
Figure 11. (a) Mean PAR ($\mu mol m^{-2} s^{-1}$) at 1600 UTC for September 2010 from DIR+DIF experiment; and (b) the mean diffuse fraction of solar radiation at 1600 UTC for September 2010 as simulated by DIR+DIF. The darker black contour line on the maps delimits the LBAR.
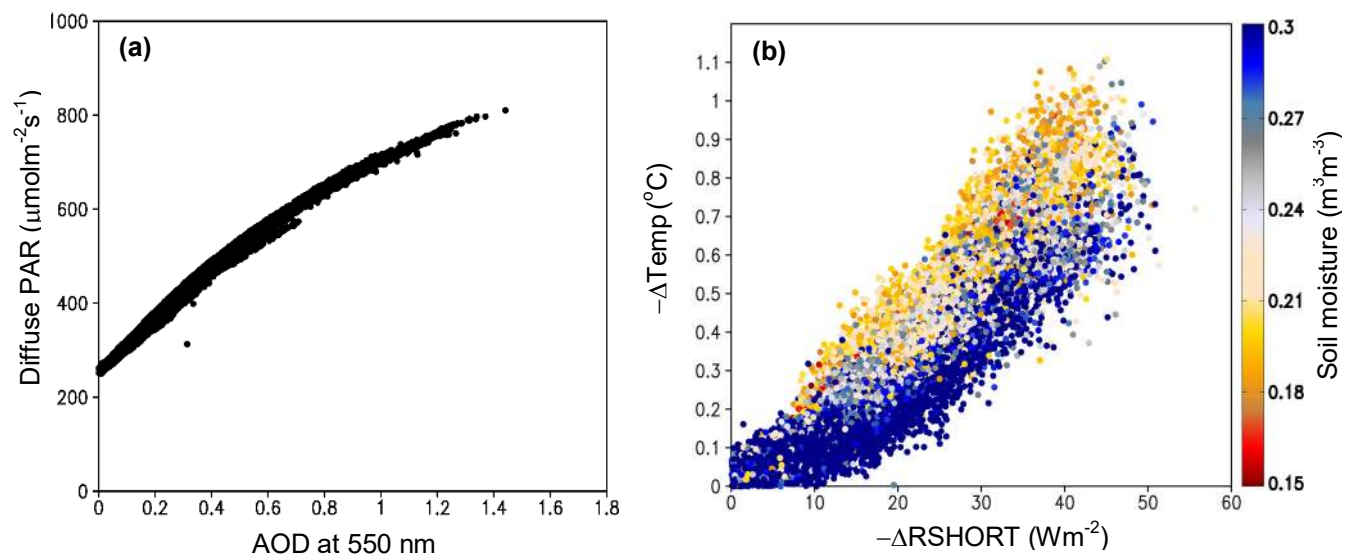
Figure 12. (a) The diffuse PAR radiance (μmolm^{-2}s^{-1}) versus AOD at 550 nm as simulated at DIR+DIF experiment at 1600 UTC during September 2010 (temporal) in the LBAR (spatial). (b) The decrease of 2-meter temperature versus the decrease of downwelling shortwave irradiance (Wm^{-2}) as simulated at AER-DIR and NO-AER experiments at 1600 UTC during September 2010 in the LBAR. The color scale refers to soil moisture (m^{3}m^{-3}) at 0.35 meter.
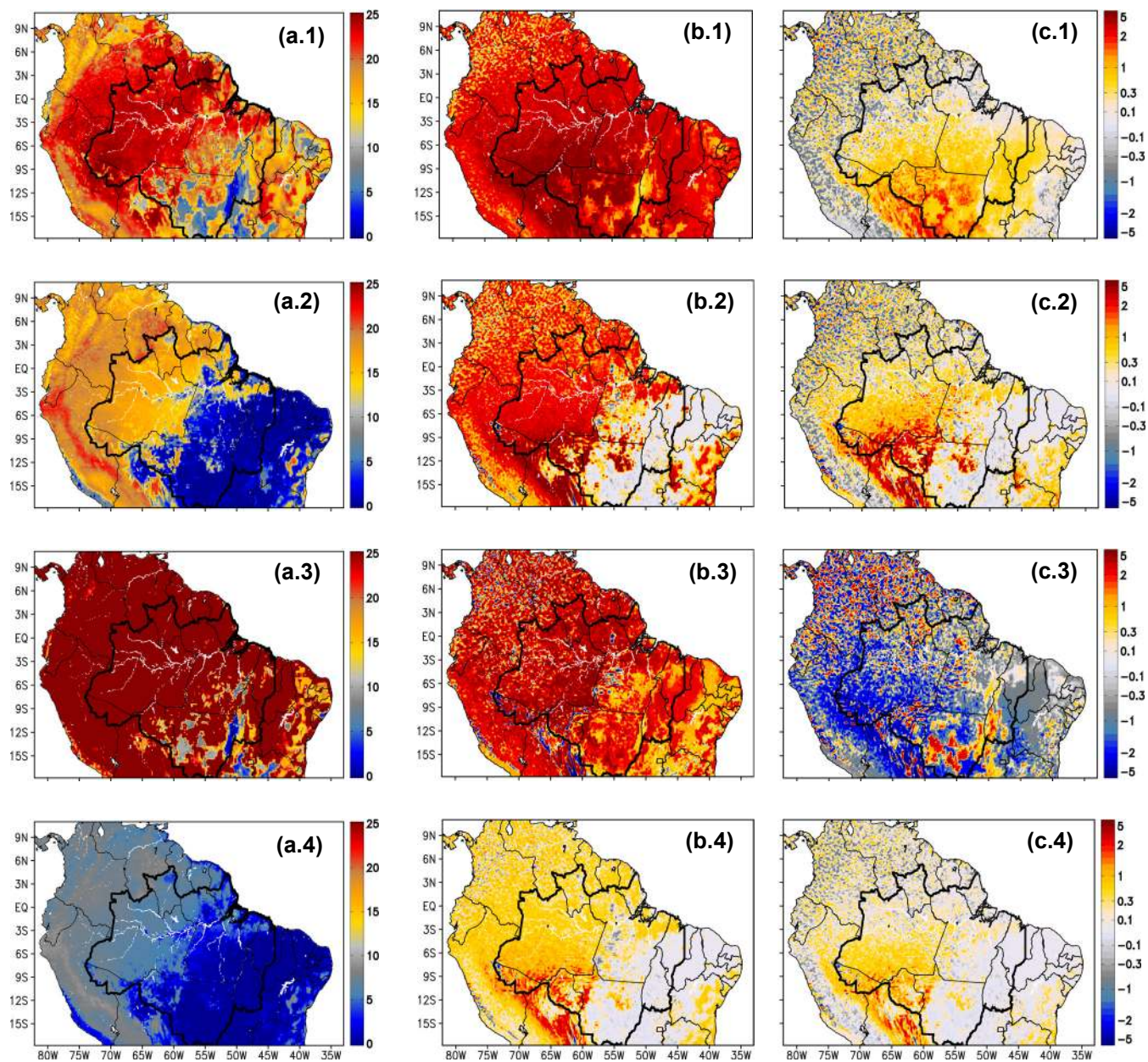
Figure 13. Mean GPP (μmolCm^{-2}s^{-1}) for September 2010 at 1600 UTC as simulated at DIR+DIF (column a), the difference in the monthly mean GPP (μmolCm^{-2}s^{-1}) as simulated at DIR+DIF and NO-AER (column b), and DIR-AER and NO-AER (column c). The lines from the 1st to the 4th present the results for the biomes of forest, C3G, C4G, and shrub, respectively. The darker black contour line on the maps delimits the LBAR.
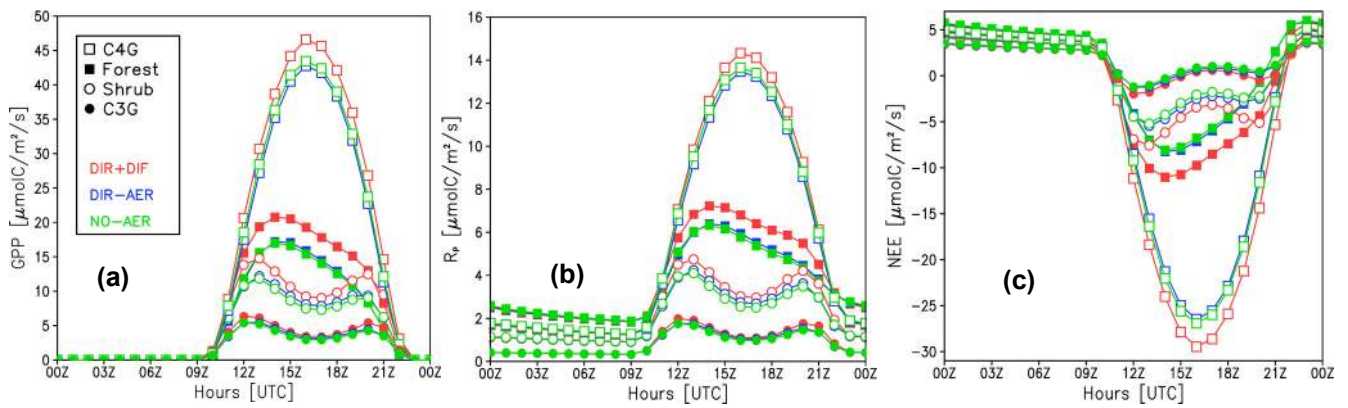
Figure 14. Mean diurnal cycle of (a) GPP (μmolCm^{-2}s^{-1}), (b) R_P (μmolCm^{-2}s^{-1}), and (c) NEE (μmolCm^{-2}s^{-1}) during September 2010 for the different biomes in the LBAR. Different symbols indicating the biomes of forest (filled squares), C3G (hollow circles), C4G (hollow squares), and shrub (filled circles); and different colors indicating the modeling experiments, green for NO-AER, blue for DIR-AER and red for DIR+DIF.
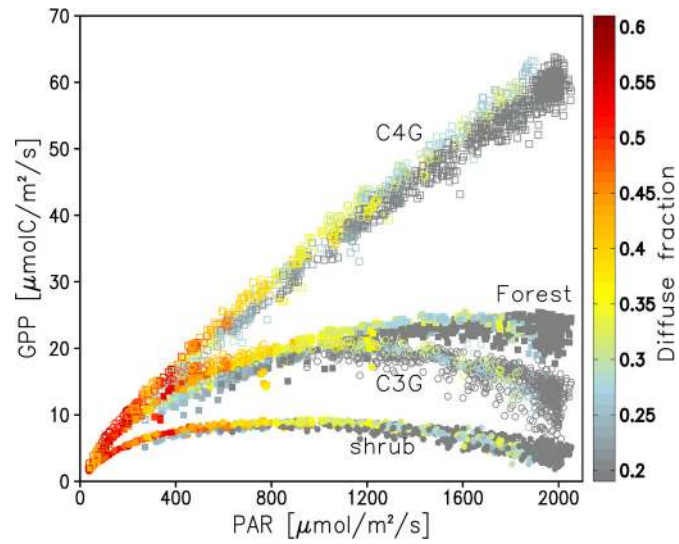
Figure 15. Figure 15: Scatter plots of GPP (µmolCm^{-2}s^{-1}) and PAR (µmolm^{-2}s^{-1}) from the DIR+DIFF experiment for forest (filled squares), shrub (filled circles) biomes, grass types C4 (hollow squares) and C3 (hollow circles) during September 2010 (temporal) in the LBAR (spatial). The color scale depicted indicates the fraction of diffuse radiation. The data were filtered for soil water factor above 0.9.
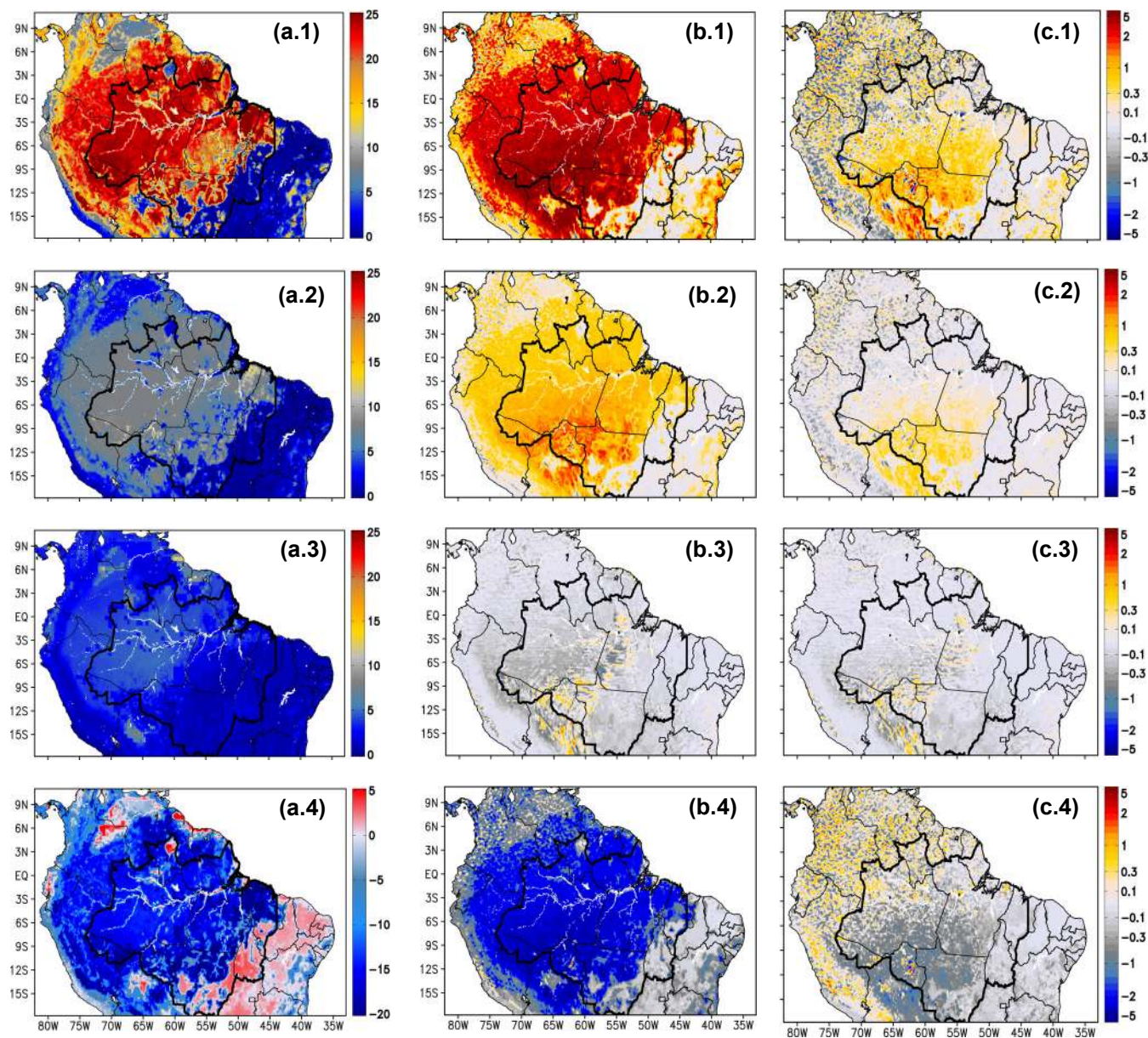
Figure 16. Mean net CO_2 fluxes (μmolCm^{-2}s^{-1}), weighted per biome type, for September 2010 at 1600 UTC (column a), and the differences in the mean CO_2 fluxes as simulated at DIR+DIF and NO-AER (column b), and DIR-AER and NO-AER (column c) during the same time period. The lines from the 1st to the 4th have the results for GPP, R_P, R_H, and NEE processes, respectively. The darker black contour line on the maps delimits the LBAR.
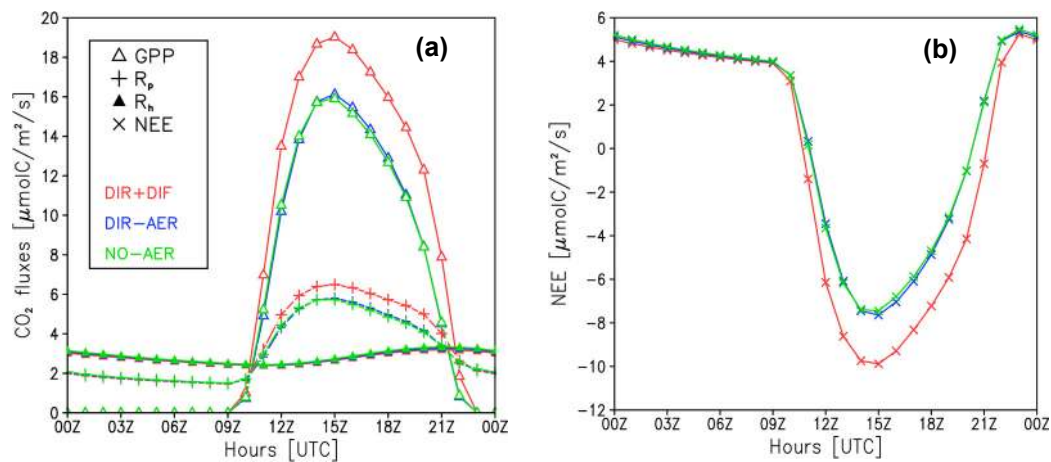
Figure 17. (a) Mean diurnal cycle of CO_2 fluxes (μmolCm^{-2}s^{-1}) during September 2010 in the LBAR, with different symbols indicating the processes of GPP (hollow triangle), R_P (plus) and R_H (filled triangles). (b) Mean diurnal cycle of CO_2 fluxes (μmolCm^{-2}s^{-1}) associated with NEE during the same period and in the same area. In both plots, different colors indicating the modeling experiments, green for NO-AER, blue for DIR-AER and red for DIR+DIF.
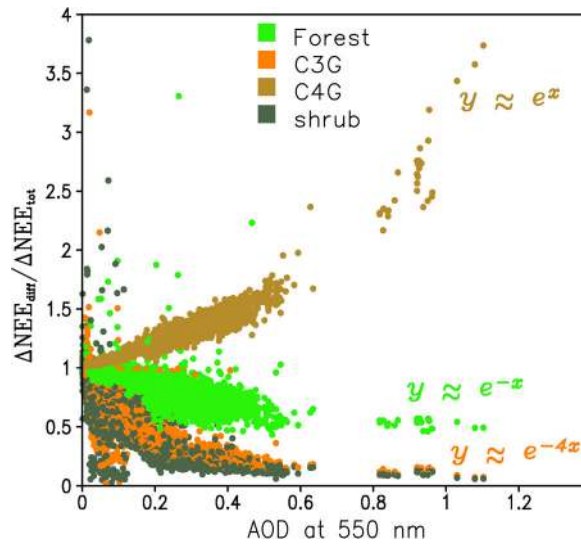
Figure 18. The contribution of the diffuse radiation effect to NEE ($\Delta NEE_{diff}/\Delta NEE_{tot}$) as a function of AOD in the LBAR, but separated with different colors for different types of vegetation. The model data were filtered for cloudiness and precipitation. Additionally, only model points with the same soil water factor within all the three experiments, and soil moisture difference below 0.001 $\mathrm{m^3 m^{-3}}$ were included. The fitting functions of the $\Delta NEE_{diff}/\Delta NEE_{tot}$ versus AOD for each biome are also shown in the figure.